Marine terrace staircases of western Iberia: Uplift rate patterns from rocky limestone coasts of central Portugal (Cape Raso - Abano beach and Cape Espichel)

António A. Martins [a], Margarida P. Gouveia [b,*] , Pedro P. Cunha [b], João Cabral [c] , Alberto Gomes [d] , Christophe Falguères [e], Pierre Voinchet [e], Martin Stokes [f], Bento Caldeira [g] , Jan-Pieter Buylaert [h,i] , Andrew S. Murray [i], Jean-Jacques Bahain [d] , Silvério Figueiredo [j]

[a] University of Évora, Department of Geosciences, ICT – Institute of Earth Sciences, Portugal
[b] University of Coimbra, MARE - Marine and Environmental Sciences Centre / ARNET, Department of Earth Sciences, Portugal
[c] University of Lisbon, Faculty of Sciences, Department of Geology, Dom Luiz Institute, Portugal
[d] University of Porto, Department of Geography, CEGOT, Portugal
[e] Sorbonne Université, Muséum National D'Histoire Naturelle, Dép. Homme et Environment, CNRS-UPVD, France
[f] School of Geography, Earth and Environmental Sciences, University of Plymouth, UK
[g] University of Évora, Department of Physics, ICT – Institute of Earth Sciences, Portugal
[h] Department of Physics, Technical University of Denmark, Risø Campus, Denmark
[i] Nordic Laboratory for Luminescence Dating, Aarhus University, Risø DTU, Denmark
[j] Polytechnic Institute of Tomar, Centro Português de Geo-História e Pré-História, Centro de Geociências – Univ. Coimbra, Portugal

ARTICLE INFO

ABSTRACT

The Western Iberian Peninsula is undergoing compressive tectonic reactivation, resulting in spatial and temporal variations of surface uplift. Uplift quantification can be undertaken in coastal settings using staircases of shore platforms developed onto rocky headlands. This study analyses two marine terrace staircases in central Portugal: Cape Raso - Abano beach and Cape Espichel. Geomorphic and stratigraphic analyses identified marine terraces/ shore platforms developed below a culminant shore platform, four at Cape Raso and eleven at Cape Espichel. The terrace chronology was obtained by using ESR and pIRIR dating. Using the interactions between the elevation, age and global mean sea-level elevations, the marine terraces were correlated with Marine Isotope Stages (MIS). The shore platforms at the Cape Espichel are more elevated than the coeval references at the Cape Raso - Abano beach and this indicates differential uplift. Considering the culminant shore platform (3.7 Ma), for the Espichel W promontory the estimated long-term uplift rate is ~0.03 m/ka, but for the Cape Raso is only ~0.01 m/ka. Also, by using the shore platform considered as produced by the MIS 15 high stand (~572 ka), the estimated uplift rate for the Espichel W promontory is ~0.13 m/ka, but for the Cape Raso is ~0.07 m/ka. The Espichel W promontory terrace staircase also allows to deduce that the estimated uplift rate was nearly constant during ~600 ka to ~200 ka ago (~0.13–0.11 m/kA), but it after decreases (~0.06–0.01 m/ka).

1. Introduction

Raised paleoshorelines, provided by shore platforms and associated marine deposits (marine terraces) are useful geomorphic markers for assessing surface uplift rate patterns along continental margins (e.g. Lajoie, 1986; Anderson et al., 1999). The present elevation of paleoshorelines results from interactions between tectonic crustal motions, eustatic sea-level fluctuations and glacial isostatic adjustment (GIA).

Global Mean Sea Levels (GMSL) are driven primarily by the growth and decay of continental ice sheets, which in turn cause changes in the volume or mass of the world's oceans (e.g. Mörner, 1982; Lajoie, 1986; Merrits and Bull, 1989; Bloom and Yonekura, 1990; Pirazzoli et al., 1993; Pedoja et al., 2014).

Sea-level changes caused by global ice sheet growth and decay ranged from ca. 22 ± 10 m (above the present sea level, a.s.l.) during part of the Pliocene (4.5–3.0 Ma) (Dowsett, 2007; Raymo et al., 2009,

2018; Miller et al., 2012, 2020; Hearty et al., 2020) to −120 (below the present sea-level) during the Last Glacial Maximum (LGM, 27 to 20 ka ago).

In rising coastal areas, the speed of surface movement (uplift rate) can be roughly expressed by dividing the amount of uplift by the time over which the crustal movement occurred, considering the sea-level change between the initial and present times (equation (1); Lajoie, 1986),

$$U = \frac{E - Sl}{T} \tag{1}$$

where U is the uplift rate, E is the present elevation of the shoreline angle of the marine terrace, SL is the eustatic sea level elevation at the time of marine terrace formation, and T is the age of the marine terrace.

Determining the age of marine terraces is always a difficult task, either due to the absence of datable material or to the complexity of the available dating methodologies. However, in terrace staircases where there are levels with some age control allowing the estimation of a local uplift rate, we may use the elevation of the undated paleo-shoreline angles and the inferred uplift-rate for estimating their age, based upon a reference paleo sea level curve (e.g. Roberts et al., 2009, 2013; De Santis et al., 2023; Robertson et al., 2023).

Despite the apparent simplicity of coastal uplift rate calculations, the extraction of this data from sea level markers (marine terraces, marine caves, corals, etc.) can be challenging due to the uncertainties associated with past eustatic levels, the scarcity of reliable numerical age control and the erosional loss of paleoshoreline evidence, especially in high-energy coastal areas. The latter case is particularly relevant on the west coast of Iberia, exposed to the high-energy conditions of the Atlantic Ocean, which result in the rapid retreat of less resistant sea cliffs, the destruction of former shore platforms and poor preservation of marine terrace deposits. In general, marine terraces in the Western Iberian Margin are rare and typically have only a small extent in rocky sea cliffs, commonly expressed as irregularly scattered remnants that are often challenging or impossible to access. However, they can be mapped using remote sensing, including unmanned aerial vehicles (drones).

There is consensus that during the late Zanclean (mid-Pliocene), a marine transgression reached up to 24 km inland from the present Portuguese coastline (Teixeira, 1979; Cunha et al., 1993; Diniz, 1984; Cachão, 1990; Ferreira, 2005; Cunha, 2019; Ramos-Pereira and Ramos, 2020), when sea level was for long time positioned at ca. 22 ± 10 m (Miller et al., 2012, 2020) a.s.l. Sediments deposited by this high sea level are expressed by a culminant sedimentary unit (allostratigraphic unit UBS13; ~3.7 to 1.8 Ma), which comprises basal beach deposits, transitioning upwards into coastal plain and fluvial sediments (Diniz et al., 2016; Cunha, 2019; Cunha et al., 2019; Gouveia et al., 2020]. The UBS13 basal unconformity is usually expressed as a regionally extensive shore platform. This platform is considered correlative to the wide shore platform of the Cantabrian Margin (NW Spain), named "Rasa" (e.g. Alvarez-Marrón et al., 2008). The top surface of the UBS13 is named the 'Littoral Platform of Portugal' (LPP; Ferreira, 1983; 1991; Araújo, 1991). The LPP has variable width on the coasts of mainland Portugal and its maximum altitude slightly exceeds 260 m inland. In some areas, deposits of uppermost Zanclean to Gelasian age form the (top) surface of the LPP, while in others the LPP is only represented by the extensive erosion surface cut in the Cenozoic, Mesozoic or Variscan substratum. The LPP is well developed along the western and southern coasts of mainland Portugal, forming a key geomorphic marker to quantify spatial and temporal variations in long-term uplift rate. River systems draining to the Atlantic coast are incised into the LPP and developed fluvial terrace staircases.

Marine terrace staircases are also cut into sedimentary bedrock or Variscan basement, at elevations below the UBS13. Attempts to date them are limited (e.g. Ramos et al., 2012; Carvalhido et al., 2014; Figueiredo, 2015; Ressurreição, 2018; Ribeiro et al., 2019). The

higher-elevation marine terraces are beyond the range of optical luminescence methods (quartz-OSL and pIRIR). Therefore, here, we use ESR dating to gain longer temporal insights, alongside the standard OSL methods.

This study focuses on two flights of marine terraces developed on the resistant limestone headlands of Cape Espichel (Espichel promontory, Chã dos Navegantes, Forte da Baralha) and Cape Raso-Abano beach area (central Portugal).

The terraces were surveyed using LiDAR data, a GPS RTK rover station, and drone surveys, which allowed measurements estimates of shoreline angle elevations of the less accessible locations of the higher and older platforms. The marine terrace geomorphology and chronology were used to: i) quantify uplift rates; ii) correlate marine terraces/shore platforms with the MISs; iii) compare the terrace staircases; and iv) discuss the uplift rates of the two coastal areas.

2. Geological and geomorphological settings

East of the Cape Espichel study area, the Arrábida Chain (~500 m max. elevation) is an Alpine orogenic fold and thrust belt composed of folded Mesozoic and Cenozoic sedimentary rocks (Ribeiro et al., 1990) (Figs. 1 and 2).

This chain is bordered by other tectonic structures such as the Albufeira Lagoon syncline to the north, the Arrábida thrust fault (ArF) to the south, and the Setúbal - Pinhal Novo fault (SPNF) to the east (Moniz, 2010). In detail, folding occurs in an ENE-WSW direction, with a few dismantled anticlines still preserved as elevations (as the São Luís and Arrábida sierras), forming cuestas and hogbacks along the north side that are cut by NW-SE and N-S faults (Fonseca et al., 2014, 2015, 2020). Minor streams with limited incision are partly controlled by these faults (Manuppella et al., 1999). Along the east side of the chain, the SPNF (a N-S to NNW-SSE left-lateral strike-slip fault) works as a transfer fault for the ArF, located to the south of the Arrábida chain (Kullberg and Kullberg, 2000, 2017, 2020; Kullberg et al., 2000).

Cape Espichel occurs at the western end of the folded chain, where strike-slip faults cut NW dipping Mesozoic rocks. Here, the culminant late Zanclean marine Cape Espichel Platform (CEP) cuts Mesozoic limestones at elevations of 120 m a.s.l. in the west, rising up to 220 m a.s.l. near Sesimbra town. The CEP is thus tectonically deformed (tilted to SW) (Daveau and Azevedo, 1980–81).

The Cape Raso and Abano beach are located near Cascais village, immediately south of an east-west trending small mountain named "Serra de Sintra" which constitutes a resistant relief carved into a Late Cretaceous igneous intrusion that reaches elevations up to 528 m.

South of "Serra de Sintra", the culminant late Zanclean shore platform is locally called Cascais Platform (CP). In this area, the CP occurs at 72–100 m a.s.l. with a gentle dip to SW, but occurs at 100–250 m a.s.l. to the north of the "Serra de Sintra", where it is displaced by NNE-SSW and N-S faults (Ribeiro, 1940; Dias, 1980; Cabral, 1995). The shore platforms that are inset below the Cascais Platform, are cut into Mesozoic limestones and sandstones. They can be found from Cape Raso to the Abano beach, ~4 km to the north. The staircase at Abano beach includes a shore platform with overlying marine sands and a shoreline angle situated at 34 m a.s.l. This terrace is a key geomorphic marker used to quantify uplift rates and is the unique that preserves enough marine deposits to perform numerical dating.

3. Previous studies

The Cape Espichel Platform (CEP) has been studied previously by several researchers (e.g., Ribeiro, 1935, 1968; Daveau and Azevedo, 1980–81; Fonseca et al., 2014). The extensive shore platform exhibits some patches of marine deposits made up of well-rounded pebbles in a coarse sandy matrix.

Topographically below the CEP, Quaternary beach deposits with consolidated sands and pebbles have been recognized on the margins of
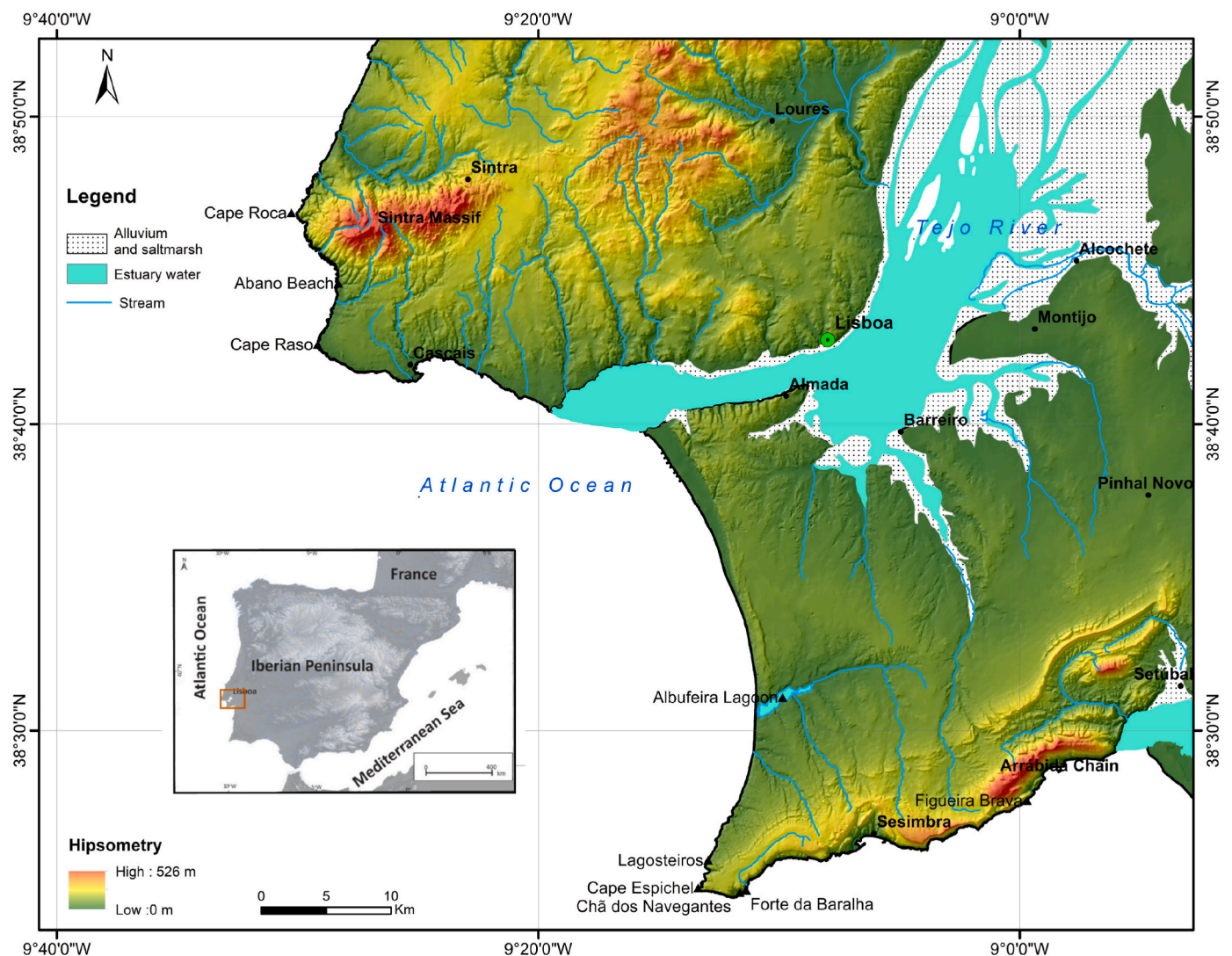
Fig. 1. Study area location map depicting the Cape Raso - Abano beach area and the Cape Espichel.

the Arrábida chain (e.g., Ribeiro, 1867; Choffat and Dollfus, 1904–1907; Breuil et al., 1942; Breuil and Zbyszewsky, 1945; Pais and Legoinha, 2000). Studies were undertaken at Lagosteiros beach (three terraces identified), Lapa de Sta. Margarida, Figueira Brava cave and Forte da Baralha (Figs. 1 and 2). In the sector between the Espichel W promontory and Forte da Baralha, cliffs were studied by Ramos-Pereira and Regnauld (1994), integrating information on emerged and submerged geomorphic features. Several raised shore platforms were mapped below the CEP, including the Forte da Baralha level (12 m a.s.l.) and a −7 m submerged level. At Forte da Baralha, several marine carbonate fragmented shells, overlying the 12 m terrace, were ^{14}C dated to 32,040 (+1410/−1190) ka cal BP and 36,786 cal BP (CalPal, 2004; Ramos-Pereira and Angelucci, 2004) or ca. 36 ka BP (Ramos-Pereira et al., 2007). The authors recognized the problem arising from the direct relationship between the ages of the shells and the marine platform on which they rest, namely the excessively high uplift rate (1.7 m/ka) resulting from this age. Such high uplift rate values are unknown on other coasts of Portugal. In our view, the ^{14}C ages obtained from fragmented shells in a coarse sand capping the shore platform should be younger than the shore platform. The marine shells were possibly transported by strong winds during the late Pleistocene, when an extensive coastal dune cover was formed along the Portuguese coast (Granja et al., 2008) and the sea level was lower than today, or it could be related to problems in the 14C datings of mollusk shells.

At Cape Espichel area, marine terraces have been identified by Cunha et al. (2015). Along this part of the coast, a flight of marine terraces is well preserved at Chã dos Navegantes, Forte da Baralha and at Espichel promontory site (Fig. 1).

At the Figueira Brava cave archaeological site (Fig. 2), the lower marine terrace is present at 6.0–7.0 m a.s.l. and has age constraints from U-series ages on speleothems and OSL ages on sediment (Zilhão et al., 2020). These ages constrain the underlying shore platform to be older than about 80–90 ka, which permits an interpretation that the platform and cave could date to MIS 5e (~125 ka).

At Cape Raso, the UBS13 is only represented by the extensive culminant shore (CP). Here, four marine terraces located below the CP have been identified (Duarte et al., 2014; Cunha et al., 2015), named Tm1 (highest) to Tm4 (lowest). At Oitavos (Fig. 3), an aeolian cover unit is largely exposed. At the base of the aeolianite succession (32 m a.s.l.), a layer of horizontally laminated muscovite rich medium sands was dated by quartz-OSL to 97 ± 4 ka (Cunha et al., 2015). Above this, there is a 1 m thick layer of fine aeolian sands containing *Helix* shells and organic matter of a paleosol, dated (^{14}C) by Monge-Soares et al. (2006) to 31, 700 + 1700 ka and −1400 ka BP. The aeolianite succession is ~10 m thick, composed of cemented coarse sands displaying dune foresets, that have been dated (using quartz-OSL) to 15-12 ka (Prudêncio et al., 2007).
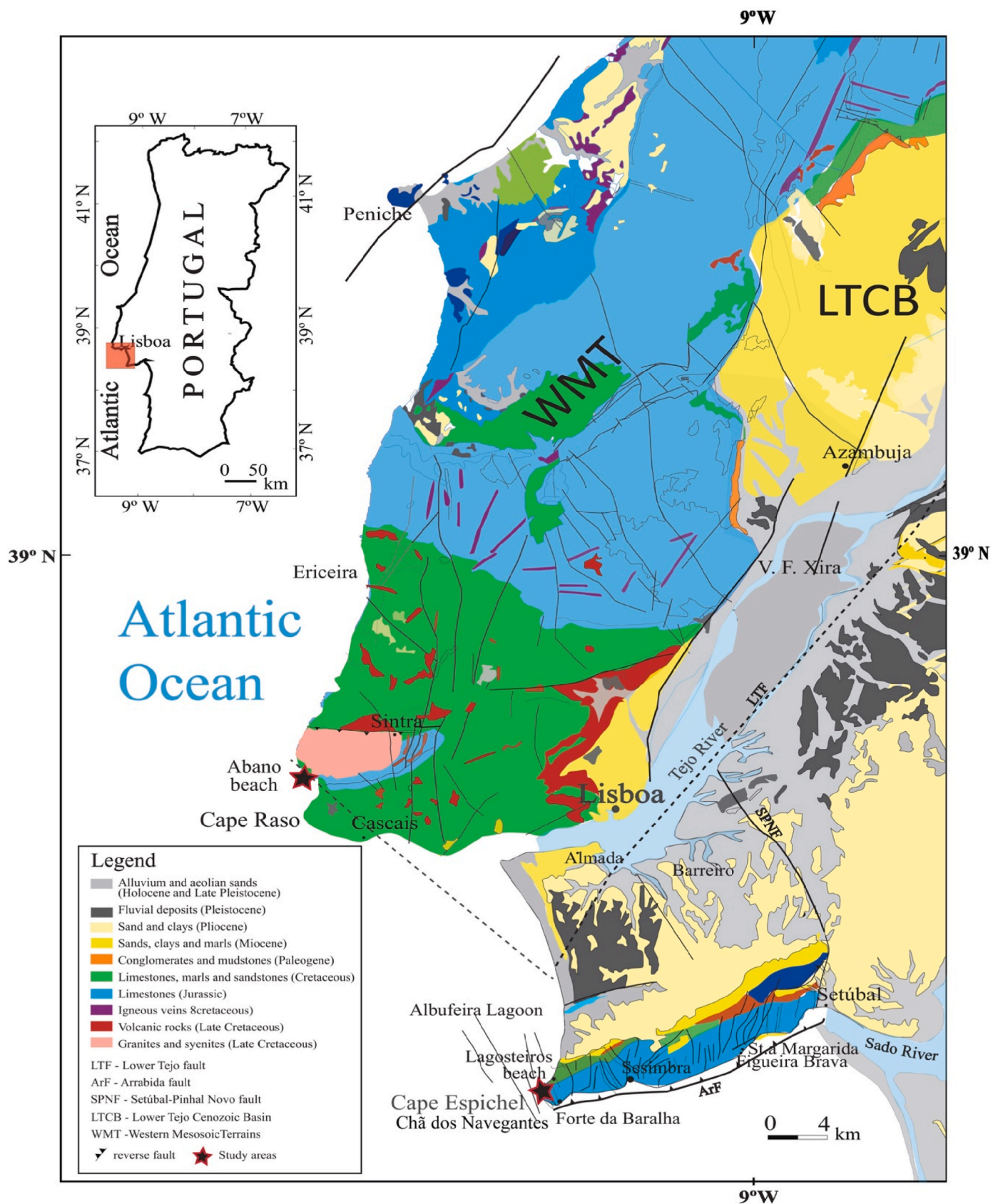
Fig. 2. Geological setting of the study area (based on the 1/500,000 geological map, LNEG).
1 – alluvium and aeolian sands (Holocene and Late Pleistocene), 2 – fluvial deposits (Pleistocene), 3 – sands and clays (Pliocene), 4 – sands, clays and marls (Miocene), 5 – conglomerates and mudstones (Paleogene), 6 – limestones, marls and sandstones (Cretaceous), 7 – limestones (Jurassic), 8 – igneous veins (Cretaceous), 9 – volcanic rocks (Late Cretaceous), 10 – granites and syenites (Late Cretaceous).
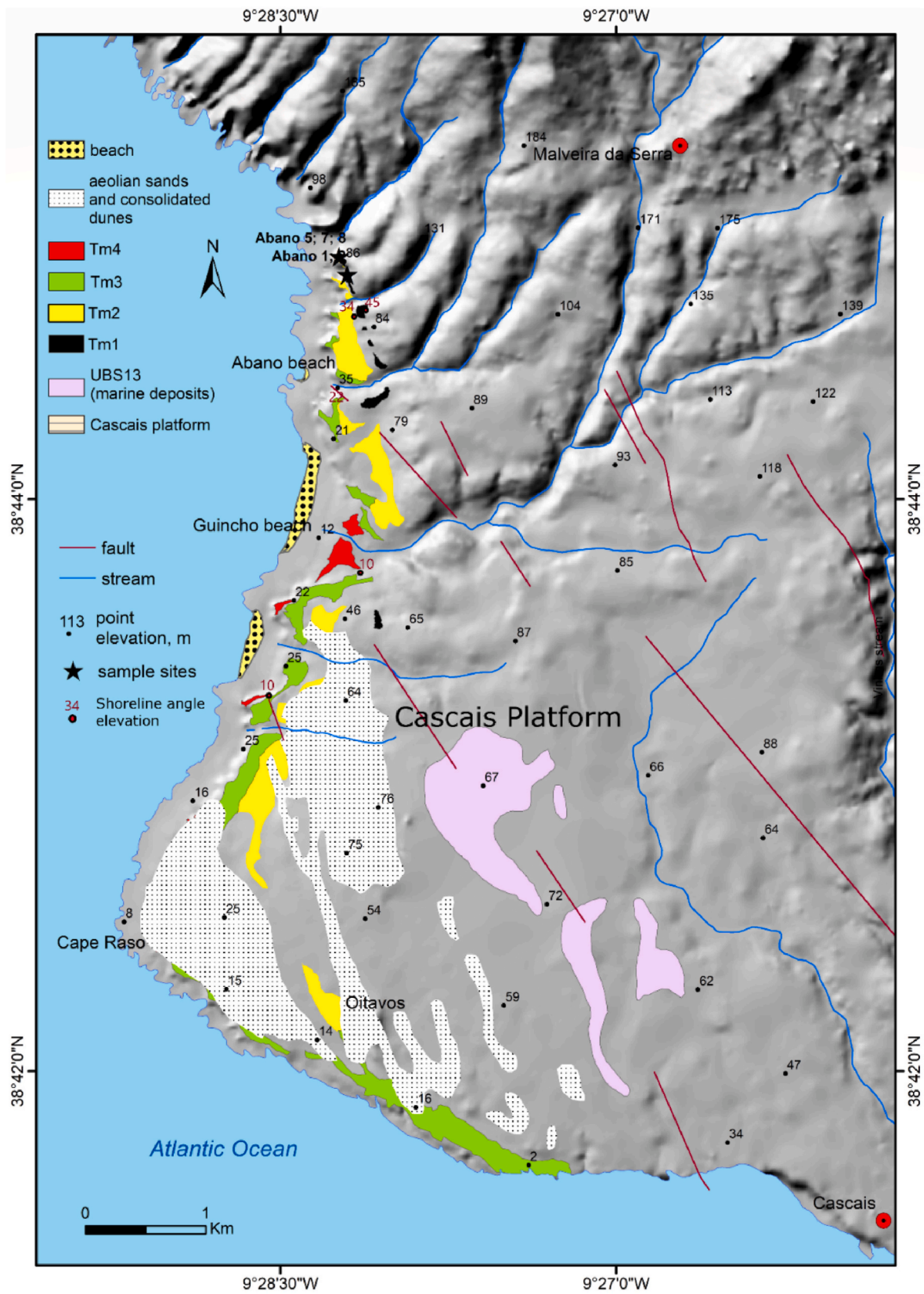
Fig. 3. Map of Cape Raso - Abano beach area, showing the Cascais Platform and the mapped marine terraces. The aeolian sand cover around Oitavos, is also shown. Shoreline angle elevations are red numbers. (For interpretation of the references to colour in this figure legend, the reader is referred to the Web version of this article.)

4. Materials and methods

4.1. Geomorphology

Geomorphological mapping was made using topographical maps at scales of 1/25000 and 1:10000 (Military Charts and municipal topographic maps), with a contour interval of 10 m and 2 m, respectively; and geological maps at 1/50000 scale (sheets 34-A, Sintra; 34-C, Cascais; 34-D, Lisboa and 38-B, Setúbal; National Laboratory of Energy and Geology - LNEG), along with high-resolution digital elevation models (DEM) based upon LiDAR data and drone surveys. LiDAR data are provided by the Portuguese Environmental Agency (APA) with mean ~30 cm vertical and 2 m horizontal resolutions. These topographic data allowed for the mapping of the marine terraces spatial distribution. The elevation of the paleo-sea level indicator, i.e., the altitude of the shoreline angle of a given marine terrace level, was measured by GPS (a GNS RTK rover station).

4.2. Sedimentology

Sedimentological analyses of the terrace deposits were performed to characterize sedimentary processes. No fossils were found. Sand grain-size analyses were carried out in the Department of Earth Sciences of the University of Coimbra (DCT-UC). The carbonate cement of sandstones was dissolved using HCl (10%). Grain-size analyses were then performed using a sieve stack with ½ Φ increments. Sand grain sediment composition analyses used binocular microscope observation (50x) and X-ray powder diffraction using a Panalytical Analytical Aeris XRD diffractometer with a Cu tube in a 2θ range, at a scanning rate of 3° min^{-1}, 40 kV and 15 nA. The mineralogical composition of non-oriented subsamples was obtained using HighScore Plus analytical software. Sand subsamples were prepared according to the standardised Panalytical backloading system, which provides near random particle distribution.

4.3. Numerical dating

At Cape Raso - Abano beach (Fig. 3), samples of marine terrace sands of the Tm2 terrace were collected in opaque tubes to prevent light exposure for electron spin resonance (ESR) and post-infrared infrared stimulated luminescence (pIRIR) dating. Samples were collected in stratigraphic order from sediments of this terrace (base at 34 m and top at 38 m a.s.l.) at ~1 m interval, labelled Abano-1 (base), Abano-5, Abano-6, Abano-7 and Abano-8 (top), respectively. Abano-6 was also used for ESR dating.

In the Cape Espichel area, the most complete terrace staircase is located at Chã dos Navegantes and the adjacent Forte da Baralha sites. In both places and at the promontory of Cape Espichel, the survey of the shoreline angle elevations of each terrace was done using the GNS RTK. Blocks of marine sandstone samples were taken for dating. Sandstone blocks were collected for ESR and luminescence dating by using a heavy hammer due to the high degree of carbonate cementation. Cores from the blocks were extracted under red light conditions, according to laboratory protocols for preventing light exposure.

The preparation of the mineral fractions was carried out in the DCT-UC, under subdued red light to avoid resetting of the luminescence signal. Each sample was wet sieved to separate the 180–250 μm grain size fraction. This fraction was treated with 10% HCl to remove carbonates, followed by 10% of H_2O_2 to remove reactive organic matter. The K-feldspar-rich fraction was separated using heavy liquid (sodium polytungstate solution; $\rho = 2.58$ g cm^{-3}) flotation. Floating grains were then etched using 10% HF acid for 40 min to dissolve the alpha-irradiated surface layer and remove surface weathering and coatings. A similar treatment was applied to the fraction $\rho > 2.58$ g cm^{-3} to obtain quartz grains, but using concentrated (40%) HF for 60 min followed by 10% HCl for 40 min in the final two stages.

Radionuclide concentrations (^{238}U, ^{232}Th and ^{40}K) were measured using high-resolution gamma spectrometry in the Nordic Laboratory for Luminescence Dating (Denmark) (Murray et al., 1987). The external beta and gamma dose rate are the same for both quartz and K-feldspar grains. For quartz, a small internal dose rate of 0.02 ± 0.01 Gy ka-1 was assumed (Vandenberghe et al., 2008). For K-feldspar grains an internal beta dose rate due to internal K (and Rb) of 0.839 ± 0.041 Gy ka-1 was used, based on X-ray fluorescence (XRF) measurements of the K-feldspar extracts (average K concentration = $12.2 \pm 0.3\%$ [n = 17]). For K-feldspar, an internal dose rate from U and Th of 0.10 ± 0.05 Gy ka-1 was assumed (consistent with Zhao and Li, 2005). The radionuclide concentrations were converted to dose rate data using the conversion factors of Guérin et al. (2011). Contributions of cosmic radiation to the dose rate were calculated following Prescott and Hutton (1994), assuming an uncertainty of 5%. The water content of each sample was estimated based on the average of the field water content and saturation water content. Equivalent doses were obtained on Risø TL/OSL DA-20 readers. Feldspar grains were mounted as medium (~4 mm) aliquots on stainless steel cups. Feldspar D_e values were measured using a post-infrared infrared stimulated luminescence (pIRIR$_{200,290}$) protocol, and the results were calculated as in Stevens et al. (2018). Dividing the D_e by the environmental dose rate (in Gy ka-1) gives the luminescence age of the sediment.

ESR dating procedure was carried out in the Dép. de Préhistoire du Muséum National d'Histoire Naturelle (MNHN), Paris. The ESR method followed the multiple center approaches (MC) and employed the standard multi-aliquot additive dose procedure, according to Duval et al. (2017) (see Supplementary Material). The ESR intensities were extracted from the spectra via Bruker WinEPR system software. Each sample was measured at least three times over several days, allowing the calculation of the mean ESR intensity and standard deviation for each measured aliquot. The equivalent dose (D_e) was determined by subtracting the residual intensity evaluated through the maximum bleaching value from the total dose. D_e was obtained by an exponential fitting function (EXP + LIN) and a single saturating exponential function (SSE) (see details in Voinchet et al., 2013) using the Microcal Origin Pro 8.1 software and weighted by the inverse of the squared ESR intensities - $1/I^2$ (Yokoyama et al., 1985), which gives greater importance to the first points.

For the age calculation, the annual dose rates received by each sediment sample were calculated by the radioelements concentrations (U, Th, and K) measured by the gamma-ray spectrometry method, and it was used the dose-rate conversion factors from Guérin et al. (2011). The grain thickness removed after HF etching was assumed to be 20 μm, and external alpha contribution was therefore considered negligible (α radiation is not considered because it is restricted to the outermost part of the sample). Values were corrected for β attenuation of spherical grains (Brennan et al., 1991; Brennan, 2003). Water content was measured by the difference in mass between the natural sample and the same sample dried for one week in one oven, and the water attenuation was based on Grün (1994). Following Prescott and Hutton (1994), the cosmic dose rate was determined based on each sample's altitude, latitude, and longitude.

4.4. Marine isotope stage correlations

The approach to ascribe a raised paleoshoreline to a specific past sea level, assumes that we actually aproximately know what sea levels were, relative to present, at various interglacials in the past. We used Spratt and Lisiecki (2016) as the main source for this and to calculate uplift rates using the paleo high sea levels, along with their proposed age assignments and terrace elevations. So, the sea level high stands (Table 1) that we used were taken from the global mean sea level curves of Spratt and Lisiecki (2016), except the other ones cited (Muhs et al., 2012; Rowe et al., 2014; Miller et al., 2020; Dumitru et al., 2021a,b).

Although the Spratt and Lisiecki (2016) paper is a superb effort at trying to decouple the eustatic and climatic components of the oxygen

Table 1

Eustatic sea-level highstands used to calculate predicted paleo-shoreline elevations, which were taken from the global mean sea level curves of Spratt and Lisiecki (2016), except the other ones cited.

MIS	AGE (Ka)	HIGHSTANDS (m a.s.l.)
MIS 1	0	0.0
MIS 5e	122	ca. 6.0 (Muhs et al., 2012)
MIS 7a	200	ca. −3.3 to 2.3 (Muhs et al., 2012)
MIS 7c	213	ca. −6.7
MIS 7e	237	ca. −9.4
MIS 9c	316	ca. −9.8
MIS 9e	323	ca. −0.6
MIS 11c	403	ca. 8.3 to 10 (Muhs et al., 2012)
MIS 11c	408	ca. 7.9
MIS 13	492	ca. −10.8
MIS 15a	572	ca. −6.6
MIS 15e	614	ca. −9.0
MIS 17	687	ca. −9.1
MIS 75	1990	ca. −1.0
MIS G1/G2	2640	ca. 6.4 (Dumitru et al., 2021a,b)
middle Pliocene	3700–2900	ca. 22 ± 10 (Miller et al., 2020)

isotope record, it is based on statistics and is really a model of what might be a sea level record. It should be noted that Table 1 shows the mean value for each high stand, later used for the estimation of uplift rates. However, their uncertainties, at two sigma, probably could reach the order of ±10 m.

In turn, for MIS 11, MIS 7a, and MIS 5e, we relied on the eustatic levels indicated by Muhs et al. (2012), because these were calculated on marine terraces levels with exceptional exposure and very well constrained through uranium series dating in coral reefs of the Curaçao island (Antilles). These MIS highstands were found to be consistent with the island's tectonic setting, which is characterized by a low uplift rate (Muhs et al., 2012).

Indeed, the highstand values for paleo-sea levels are still under discussion, namely for the effect of the glacial isostatic adjustment (GIA) (Creveling et al., 2015, 2017); however, the study area can be considered as not affected by GIA. An example of an area not affected by GIA is the Canary Islands (just south of this study area) where the paleo-sea level at MIS 5e is predicted to be +5 to +8 m a.s.l. (Muhs et al., 2014).

5. Results

5.1. Geomorphology and sedimentology of the Cape Raso terrace staircase

At Cape Raso-Abano beach, four marine terraces located below the Cascais Platform (CP; 72–100 m a.s.l.) have been identified, labelled Tm1 (uppermost) to Tm4 (lowermost) (Fig. 3; Table 2).

Tm2 has a sediment thickness enabling sampling for ESR and OSL dating; no fossils were found. The other terraces (Tm1, Tm3 and Tm4) are mainly rocky shore platforms, without enough sedimentary thickness for this type of dating.

The Tm1 terrace (38–45 m a.s.l.) is represented by remnants of a shore platform, below the CP. Scattered rounded boulders can be found on this terrace level.

Table 2

Summary of the marine terraces of the Abano beach.

Terrace	Paleoshoreline angle, (m)	Sedimentary cover/or rocky platform	Sample
Tm1	45	boulders and cobles	-
Tm2	34	gravels and coarse to medium sands, overlying a shore platform	Abano-1 Abano-5 Abano-6 Abano-7 Abano-8
Tm3	22	shore platform	-
Tm4	10	shore platform	-

Tm2 is situated at 34–37 m a.s.l. at Abano beach, and at 25–34 m a.s. l. further south at Cape Raso. The Tm2 shore platform is covered with siliciclastic boulders, pebbles, and coarse beach sands.

Tm3 forms a narrow surface strip developed into the limestone substrate; it rises from 16 m at Cape Raso up to 22 m in the Abano beach area.

Tm4 is recognized only to the South of Guincho beach. Remnants of this terrace form a very narrow and discontinuous strip at 9–10 m a.s.l., cutting the limestone layers.

The Tm2 sedimentary sequence used for dating is located north of Abano beach, where the shoreline angle was measured at 34.0 m a.s.l. The deposits comprise basal gravels with rounded boulders and pebbles, overlain by coarse to medium sands, collectively considered to be of beach genesis. These gravels and sands are overlain by sandy colluvium at the top. The Abano-6 sample was collected from the middle part of the terrace sedimentary sequence. The sample has an orange colour (7.5 YR 5/6), and a mean grain size of 0.5 mm (coarse-medium sand). Grain-size analysis reveals an almost symmetric distribution, dominated by medium to coarse grain sand. The average grain-size fractions consist of sand (97.8%), silt (1.8%) and clay (0.4%). The sediment is fine skewed (0.6), mesokurtic (2.64) and very poorly sorted (2.62). The sand fraction is composed of hyaline quartz (80%), feldspars (15%) and some dark minerals. The quartz grains are rounded to sub-rounded.

5.2. Geomorphology and sedimentology of the Cape Espichel terrace staircase

In the Cape Espichel area (western promontory, Chã dos Navegantes and Forte da Baralha sites) eleven marine terraces, Tm1 to Tm11, are found at elevations between 109 m and 7 m a.s.l. (Table 3), inset below

Table 3

Paleoshoreline angle elevations and typology of the marine terraces at the promontory of Cape Espichel. Sediment samples not dated are indicated by (N). All conglomerates consist of rolled limestone clasts, except one of sandstone found on Tm8.

Reference	Paleo-shoreline angle elevation (m)	Sedimentary cover/or rocky shore platform	Sample
CEP	120	rocky platform with remains of marine sands embedded into the platform surface at 120 m	–
Tm1	109.0	small shore platform	–
Tm2	91.0	small shore platform	–
Tm3	83.0	cemented marine gravels at the base and very coarse sand at the top (~90.0 m a.s.l.).	Espi-10 (N)
Tm4	74.4	cemented marine gravels at the base, followed by very coarse sandstones and colluvial deposits at the top	Espi-11 (N)
Tm5	68.0	basal conglomerate followed by sandstones and a thin layer of cemented colluvial deposits at the top (~5 m thick; top surface at ~73.0 m)	Espi-5 (pIRIR)
Tm6	53.4	basal boulder conglomerate followed by very coarse sandstones and a thick layer (~5 m) of cemented colluvial deposits at the top ~4 m thick; top surface at ~57.5 m	Espi-4 (pIRIR) Espi-8 (ESR)
Tm7	45.0	cemented colluvial deposits.	
Tm8	33.6	basal boulder conglomerate with cemented colluvial deposits at the top (~9.0 m thick)	Espi-7, a sandstone boulder (ESR)
Tm9	27.0	rocky shore platform	
Tm10	12.0	rocky shore platform	
Tm11	7.0	rocky shore platform	
modern	2.0	rocky shore platform	

the CEP (Figs. 4–7). On the cliffs at the western promontory of Cape Espichel, the shore platform remnants have a very restricted distribution; however, cemented beach sands and gravels can be found embedded into the paleo sea cliffs at different altitudes (Table 3 and Fig. 4); no fossils could be identified.

The marine platforms located below Tm8 are difficult to recognize in the western end of Cape Espichel due to cliff erosion, with the two lowermost levels being dangerously inaccessible. However, by combining the analysis of the LIDAR data, the drone topographic survey and lateral correlation with the platforms at the nearby Forte da Baralha and Chã dos Navegantes sites, we were able to map three marine terrace levels below the Tm8: Tm9 at 27.0 m; Tm10 at 12.0 m and Tm11 at 7.0 m.

The shore platforms are well developed in the Chã dos Navegantes cove (Fig. 5), but sedimentary deposits are lacking on almost all platforms, making numerical dating impossible. At Forte da Baralha, the Tm10 terrace, with a shoreline angle at 12.0 m, has beach sandstones which were not dated in this study. Given the proximity of the Chã dos Navegantes and Forte da Baralha sites, the terraces are presented together in Table 4.

On the promontory of Cape Espichel (Fig. 4), the samples for dating were collected from the Tm5 terrace (shoreline angle at 68.0 m), Tm6 (shoreline angle at 53.4 m) and Tm8 (shoreline angle at 33.6 m).

The sample Espi-7 was collected from Tm8 at ~36 m a.s.l., from a boulder of sandstone, composed of pebbly medium sand, with a light grey colour (7.5 YR 8/3) and carbonate cement. The mean grain size is dominated by coarse sand (0.67 mm) with a unimodal (0.55 mm) size. The grain-size fractions consist of sand (98.3 %) and gravel (1.7 %). The sediment is moderately sorted (0.9), leptokurtic (3.86) and fine skewed (0.7). The quartz grains are subangular.

Samples Espi-4 and Espi-8 were collected from the middle-upper part of Tm6 (at 56 m a.s.l.). These beach sandstone samples have a dull orange colour (7.5 YR 7/4), with calcium carbonate cement. The mean grain size is dominated by coarse sand (0.59 mm), is unimodal (0.50 mm) and moderately sorted (1.03) with a fine skewness (0.84). Inspection of quartz grains from the 180–250 μm fraction reveals a cover of manganese oxides for some grains.

Sample Espi-5 was collected in the middle part of Tm5 (68.0 m a.s.l.) and is a coarse sandstone.

5.3. Results and discussion of ESR and OSL dating

Regarding the results of samples taken for ESR dating (Tables 5–7), the dating from the Al centre could be measured for all samples, but from the Ti-Li centre it was not possible to measure the sample Espi-8 (Table 6). In this case, the signal intensity was too different from each measurement to be reliably evaluated, even with two scans. This contrasts, for example, with sample Espi-7, for which the use of a multi-centre approach was possible. Here, bleaching mean values are between 40 and 67%.

For Ti-Li, the equivalent dose (D_e) was determined following different approaches: the exponential and linear fitting function (Duval et al., 2009; Voinchet et al., 2013), the single saturating exponential function by limiting the curve to the first six points (from natural to 4000 Gy) and the double saturation exponential function (Fig. SM1 in Supplementary Material).

5.3.1. Cape Raso – abano beach site

All dated samples from the Abano beach site (both ESR and pIRIR) belong to Tm2 (local shoreline angle at 34.0 m a.s.l.), comprising a sedimentary sequence of a basal level of rounded gravels, intermediate coarse beach sands (samples Abano-1, -5, -6 and -7) and a sandy colluvium at the top (Abano-8) (Tables 5–7; Figs. 8 and 9). The obtained ESR ages: The age of Abano −1 (>590 ka) allows to consider an age of ca. 600 ka with a coeval sea-level peak of −7 m for the shoreline angle of Tm2 (Table 1); for Abano-5 are 520 ± 51 ka (Ti-Li) and 529 ± 48 ka
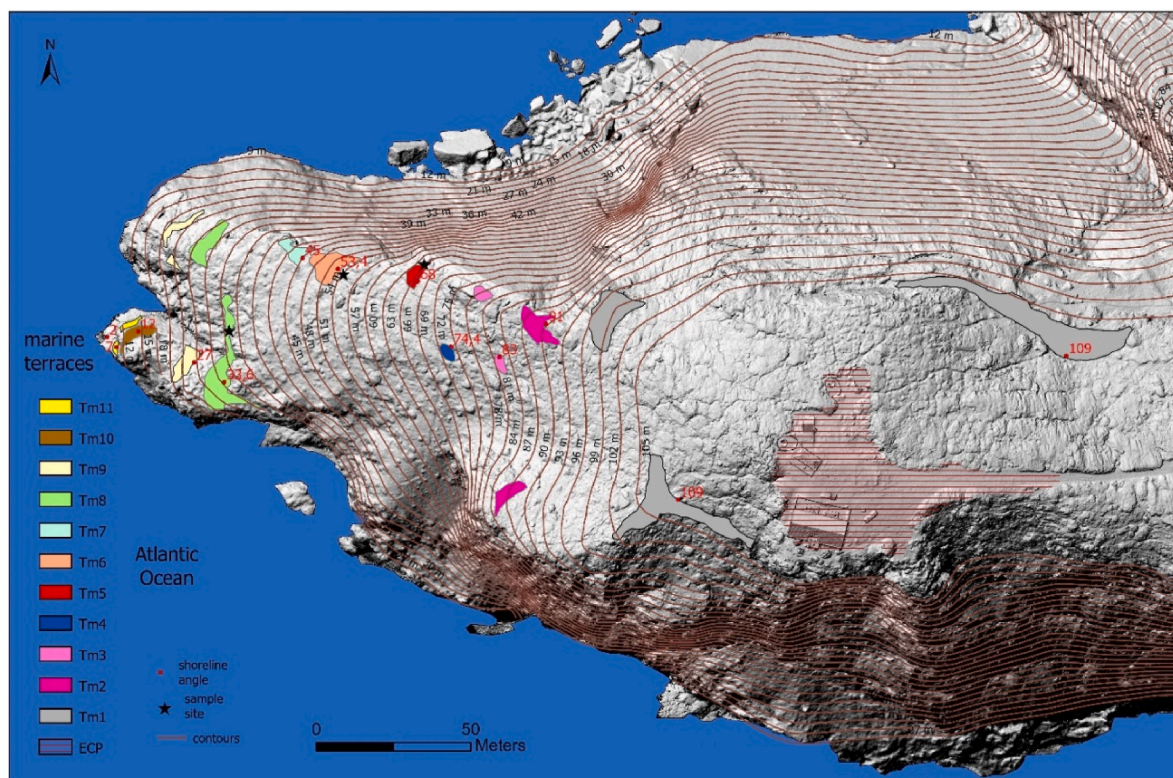
Fig. 4. The terraces staircase at the western promontory of Cape Espichel. Eleven emerged marine terraces were recognized. Some terraces, without geomorphological expression, were identified by the sedimentary record on the steep slope of the headland. Red numbers indicate the shoreline angle elevations. (For interpretation of the references to colour in this figure legend, the reader is referred to the Web version of this article.)
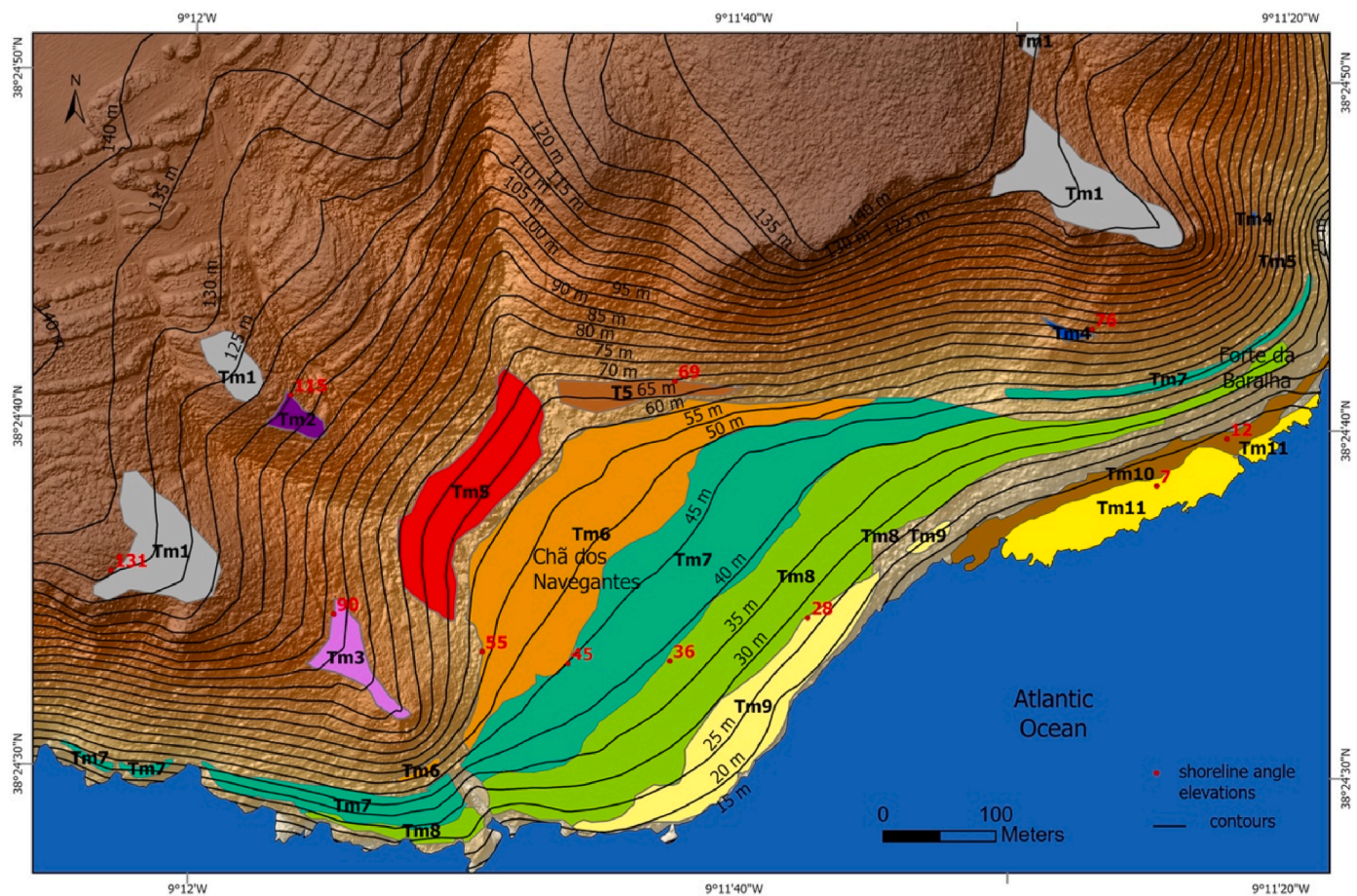
Fig. 5. Geomorphological map of the Chã dos Navegantes and Forte da Baralha sectors. Eleven emerged marine terraces and one submerged terrace (at −7 m) were recognized. The Tm10 (12 m) has a sedimentary record, but most of the shore platforms have insufficient sediment thickness for numerical dating. Red numbers represent shoreline angle elevations. (For interpretation of the references to colour in this figure legend, the reader is referred to the Web version of this article.)
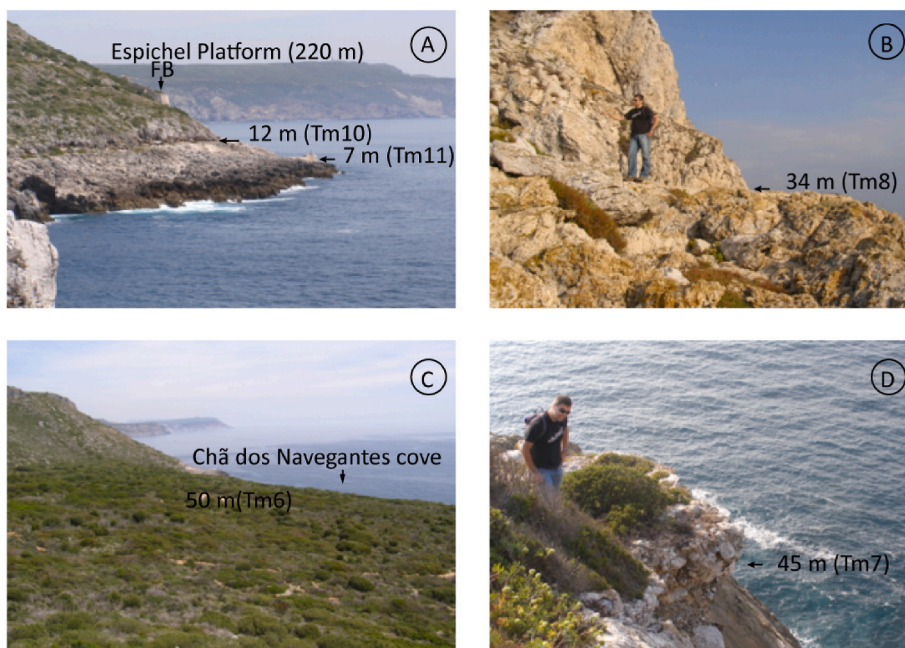
Fig. 6. A – Forte da Baralha ruins (FB) and the shoreline angles (a.s.l.) of the Tm10 (12 m) and Tm11 (7 m); B – paleo-shoreline angle of the Tm8 terrace (34 m); C – the Chã dos Navegantes cove; D – rolled limestone boulders of the Tm7 terrace (45 m).
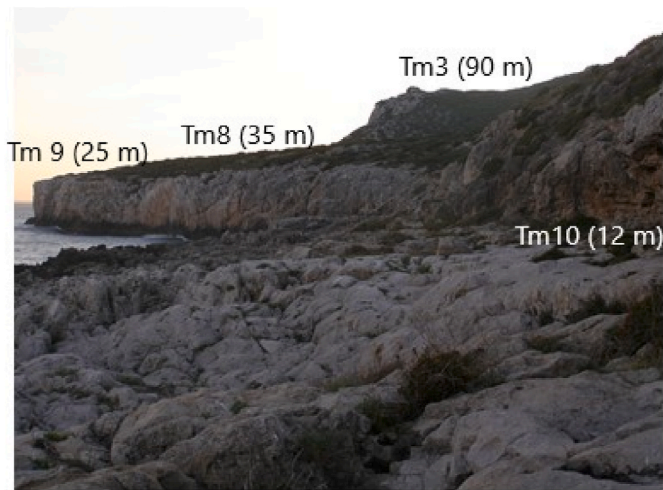
Fig. 7. Panoramic view taken from the shore platforms of the Tm10 at Forte da Baralha to the Chã dos Navegantes. Several marine platforms can be distinguished: the Tm10 (12 m), Tm9 (25 m); Tm8 (35 m) and Tm3 (90 m).

Table 4
Paleoshoreline angle elevations and typology of the marine terraces at the Chã dos Navegantes - Forte da Baralha sector.

Level	Shoreline angle elevations (m)	Sedimentary cover/rocky shore platform	Sample
CEP	145	shore platform, with rare remains of rounded pebbles and sands	–
Tm1	131	shore platform	–
Tm 2	115	shore platform	–
Tm 3	90	shore platform	–
Tm 4	76	shore platform and cemented marine pebbles	–
Tm 5	69	shore platform, scattered round pebbles	–
Tm 6	55	shore platform, scattered round pebbles	–
Tm 7	45	shore platform	–
Tm 8	36	shore platform	–
Tm 9	28	shore platform	–
Tm10	12	shore platform with marine deposits	–
Tm 11	7	shore platform	–
Modern	2	shore platform	–
Tm12	−7	submerged shore platform (Equipa ERLIDES, 1992)	–

(Al); for Abano-6 are 433 ± 66 ka (Ti-Li) and 416 ± 42 ka (Al). The pIRIR measurements of Tm2 samples provided only minimum ages ranging from >440 to >590 ka, discarding correlation with MIS 11 (younger) and MIS12 (low sea level). The ESR samples gave ages similar to the pIRIR minimum ages (signal near saturation) of Abano-6. Considering the ages of all Abano beach samples, the Tm2 sedimentation should span from MIS 15 (620–570 ka). An uplift rate of ~0.07m/ka (41m/600ka) is obtained for this coastal stretch and can be used to estimate the ages of the other marine terraces of this staircase.

For the attribution of a paleo sea-level and the attribution of the other terraces to a MIS the following procedure was used.

1) We dated Tm2, and the obtained ages (Fig. 8) indicate that the Tm2 marine terrace should have be formed during MIS 15 (620 - 570 Ka);
2) Using the sea-level curve of Spratt and Lisiecki (2016), we calculated a local uplift rate from Tm2 by evaluating the vertical offset between the sea-level at the time of the Tm2 formation (-7m, according to Spratt and Lisiecki, 2016) and the current position of the terrace shoreline angle;
3) Assuming a uniform uplift rate of 0.07 m/ka, and using again the Spratt and Lisiecki sea level curve, we assigned a marine isotope stage and an age to all other undated terraces, based on a best fit between the expected and the actual terrace sequence.

The Tm1 (42.0 m a.s.l) was ascribed to MIS17 because of its higher elevation with respect to Tm2 and because, using the uplift rate rate of 0.07 m/ka, an estimated age of 729 ka is obtained, which is compatible with the MIS17 (710 -680 ka).

According to Spratt and Lisiecki (2016), sea levels were lower during MIS 13 (about −11 m at 492 ka, and −14 m at 498 ka). Using these eustatic sea level values and an uplift rate of 0.07 m/ka, estimated ages of 471 and 514 ka were obtained for the Tm3 (at 22.0 m a.s.l.). This implies that Tm3 may represent the MIS 13 (533–478 ka) and could have been reoccupied during the MIS 9e (323 ka), when the sea level was at ca.-0.6 m. The correlation of the Tm3 with the MIS 11 (403 ka; +9 m) is not possible as for the assumed uniform uplift rate of 0.07 m/ka the correlative marine terrace should be at a much higher elevation of ca. 37 m; so, we have to admit that the MIS 11 is not recorded in the Raso Cape - Abano beach staircase.

For the Tm4, with a shoreline angle located at 9.0 m a.s.l., a correlation with the MIS 7 (coeval sea-level peak of 2.3 m; 200 ka) is only possible by using an estimated uplift rate of 0.03 m/ka. The Tm4 should not be correlated with the MIS 5e (coeval sea-level peak of 6.0 m; 122 ka), because this would imply an even lower uplift rate of 0.02 m/ka.

So, if we assume a uniform uplift rate of 0.07 m/ka we conclude that the MIS 5e level should be at a height of ca. 8.5 m and thus is not recorded in the Cape Raso area. It was probably eroded by the Holocene high stand, as is the case along other stretches of the Portuguese coast (Ramos-Pereira, 2008; Araújo, 2008, 2020; Figueiredo et al., 2013; Zilhão et al., 2020).

5.3.2. Cape Espichel promontory

For the terrace staircase located at the Cape Espichel promontory, several paleobeach sandstones, collected from different terrace levels yielded numerical ages. The following terrace deposits were dated (Figs. 10 and 11).

- From Tm5 (shoreline angle at +68.0 m), a sample (Espi-5) collected at the base of the sandstone unit yielded a pIRIR minimal age of >450 ka, but also ESR ages of 598 ± 139 ka (Ti-Li) and 646 ± 58 ka (Al), encompassing MIS 15 (620 - 570 ka). The upper level of the sandstone (>450 ka) could correlate with MIS 13 (520 - 470 ka), however, it should be noted that this latter age is a minimum.
- From Tm6 (+53.4 m), sample Espi-4 gave a pIRIR age of >420 ka and ESR ages of 432 ± 48 ka (Ti-Li) and 405 ± 64 ka (Al); sample Espi-8 provided a pIRIR age >430 kA and ESR (Al) age of 343 ± 10 ka. This allows correlation with MIS 11 (430 - 360 ka).

Table 5
Dosimetry and ESR in Al, Ti−Li centre of collected marine terraces sedimentary samples.

Sample code	U(ppm)	Th(ppm)	K(%)	D''β (μG/a)	Dcos (μG/a)	Dγ (μG/a)	Dt (μG/a)	Wc (%)
Abano-5	0.98 ± 0.06	3.21 ± 0.4	1.081 ± 0.05	887 ± 25	124 ± 7.5	473 ± 34	1510 ± 58	10
Abano-6	0.65 ± 0.06	2.38 ± 0.4	0.49 ± 0.02	422.1 ± 23.7	76.1 ± 3.8	274 ± 27	772 ± 36	10
Espi-4	0.49 ± 0.06	1.48 ± 0.3	1.19 ± 0.09	870 ± 25.0	166 ± 8.0	375 ± 39	1423 ± 41	10
Espi-5	0.51 ± 0.06	1.84 ± 0.30	0.96 ± 0.08	727 ± 13	190 ± 9.0	341 ± 36	1273 ± 39	10
Espi-7	0.29 ± 0.06	0.75 ± 0.07	0.74 ± 0.01	535.4 ± 16.8	163.8 ± 8.1	243.8 ± 5.1	965 ± 14	5
Espi-8	0.61 ± 0.08	1.86 ± 0.10	2.56 ± 0.02	1799 ± 16	164.8 ± 9.1	733.6 ± 17.6	2.691 ± 19	7

Table 6
ESR age of sedimentary samples collected from the marine terraces.

Sample code	Depth (m)	Elevat. (m)	Grain size (μm)	Bleaching (%)	De Ti-Li (Gy)	Adj. Square	De Al (Gy)	Adj. Square	Age (ka) Ti-Li	Age (ka) Al
Abano-5	2.8	34.4	100–200	52	786 ±9	0.97	799 ±87	0.99	520 ±51	529 ±48
Abano-6	0.6	35.0	300	58	334 ±48	0.99	321 ±29	0.99	433 ±66	416 ±42
Espi-4	1.0	57.5	250–180	56	616 ±54	0.98	576 ±65	0.97	432 ±48	405 ±64
Espi-5	0.1	70.0	250–180	54	762 ±61	0.99	823 ±77	0.98	598 ±39	646 ±58
Espi-7	0.2	36.0	250–180	48	581 ±31	0.98	573 ±60	0.99	618 ±34	609 ±64
Espi-8	0.1	56.0	250–180	50	–	–	723 ±25	0.99	–	343 ±10

Table 7
Post-IR IRSL ages of samples collected from Cape Raso - Abano beach and Cape Espichel marine terraces. Samples with measured De values significantly greater than 900 Gy are given as minimum ages, because the accuracy of palaeodoses >1000 Gy has not been established with confidence yet.

Sample code	Elevation (m)	Grain size (μm)	pIRIR (De Gy)	N° cups	Dose rate (Gy/ka)	Age (ka)
Abano-1 052233	30.0	250–180	>1000	11	1.70 ± 0.06	>590
Abano-5 072217	34.4	250–180	>1000	6	2.22 ± 0.08	>450
Abano-6 072218	35.0	250–180	>1000	6	2.25 ± 0.08	>440
Abano-7 072219	35.5	250–180	>1000	3	2.33 ± 0.73	>430
Abano-8 072220	36.5	250–180	>1000	4	5.62 ± 0.19	>180
Oitavos 052232	31.0	250–180	182 ± 5	6	2.45 ± 0.10	74 ± 4
Espi-4 052243	54.0	250–180	>1000	5	2.37 ± 0.08	>420
Espi-5 052241	69.0	250–180	>1000	3	2.23 ± 0.11	>450
Espi-7 202228	36.0	250–180	>1000	6	2.25 ± 0.08	>440
Espi-8 202229	56.0	250–180	>1000	6	2.31 ± 0.08	>430

- Tm7 only records a colluvium, not a marine sediment, for that reason, this terrace level was not dated.
- Tm8 (+33.6 m) provided a rounded boulder of sandstone (Espi-7) that yielded ESR ages of 618 ± 34 ka (Ti-Li) and 609 ± 64 ka (Al), but also a pIRIR age >440 ka. This boulder should represent a sandstone fallen from the cliff; so, Tm8, being a marine terrace located immediately below Tm6 and Tm7 could represent MIS 9e (323 ka).
- Tm9 (+27.0 m) is represented by a very narrow shore platform, probably corresponding to MIS 9c (316 ka).
- Tm10 (+12.0 m) is represented by shore platform, probably corresponding to MIS 7 (240 - 180 ka).
- Tm11 (+7.0 m) should be correlated with the shore platform located at the nearby Figueira Brava archaeological site, with a paleo-shoreline angle at 7.0 m a.s.l. and associated marine deposits which was were attributed to the MIS 5e (Zilhão et al., 2020).

Considering the long-lasting period of the CEP formation, from the upper Pliocene until the Lower Pleistocene, we admit that the terraces Tm1 to Tm4 were formed during the Middle Pleistocene Transition (MPT; 1.2 to 0.7 Ma). Tm4 and Tm3 could be correlated with MIS 17 and MIS 19, respectively.

From the described marine terraces, the respective uplift rates could be estimated.

- For Tm5, with a coastal angle at 68.0 m a.s.l., considering a coeval sea level peak of −6.6 m (MIS 15a highstand, 572 ka; Table 1), the uplift rate is ~0.13 m/ka;
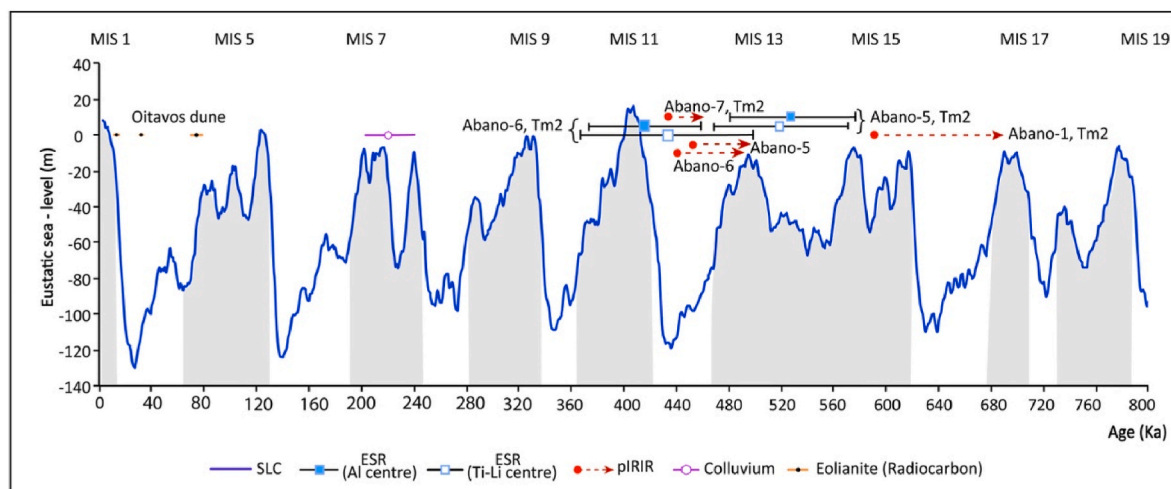
Fig. 8. Ages given by the samples measured by pIRIR (minimum) and ESR methods, collected from the sands of the Tm2 terrace in the Abano beach (Cape Raso area). Eustatic sea level curve data from Spratt and Lisiecki (2016).
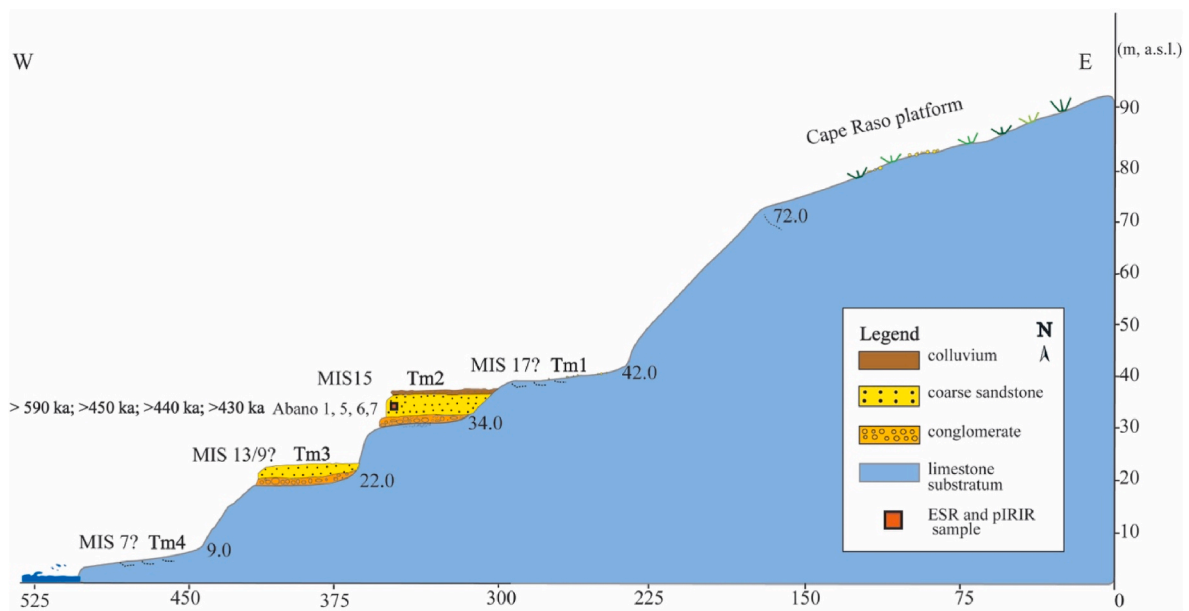
Fig. 9. – Schematic cross profile of the terrace staircase at the Cape Raso - Abano beach area.
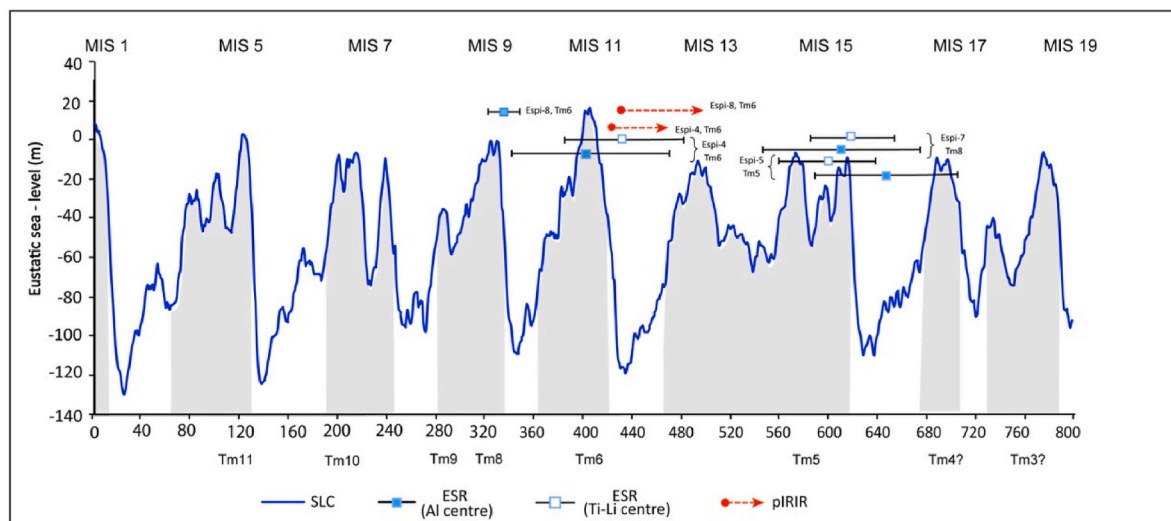
Fig. 10. Age results derived from pIRIR (minimum) and ESR methods in the Cape Espichel promontory. Eustatic sea level curve data from Spratt and Lisiecki (2016).

- For Tm6 (+53.4 m), considering a coeval sea level peak of +9 m (MIS 11c highstand, 403 ka), the uplift rate is ~0.11 m/ka;
- For the Tm7 (+45 m) considering a coeval sea level peak of ca. −11m for the MIS 13 highstand, (492 ka), the uplift rate is 0.11m/ka.
- For Tm8 (+33.6 m), considering a coeval sea level peak of −0.6 m (MIS 9e highstand, 323 ka), the uplift rate is ~0.11 m/ka;
- For Tm9 (+27.0 m), considering a coeval sea level peak of −9.9 m (MIS 9c highstand, 316 ka), the uplift rate is ~0.12 m/ka;
- For Tm10 (12.0 m), considering a coeval sea level peak of ~0 m (MIS 7a highstand, 200 ka), the uplift rate is 0.06 m/ka;
- For Tm11 (+7.0 m), considering a coeval sea level peak of +6.0 m (MIS 5e highstand, 122 ka), the uplift rate is 0.01 m/ka;

6. Discussion

Despite the inherent uncertainties in eustatic levels, at the Cabo Espichel promontory, the reasonable matching of coastal terrace angles with the different MISs suggests that the tectonic uplift rates (between 0.11 and 0.13 m/ka) are likely close to the true values for the period from MIS 17 to MIS 7. After MIS 7, the tectonic uplift rate seems to have decreased considerably.

The large extension of the Cape Espichel Platform (~10 km westward of Sesimbra town), carved on the resistant limestones of the Arrábida Chain, implies that the development of this shore platform occurred over an extended period. It occurs at 120 m on the west end of Cape Espichel but reaches 220 m a.s.l. towards the ENE, suggesting a slight tilt of the platform due to differential vertical displacement by active tectonics.

By 3.7 Ma, the eustatic sea level reached +22 m (Miller et al., 2020). Considering the CEP altitude at its western edge (120 m), we obtain a long-term uplift rate of 0.03 m/ka at this location in the last 3.7 Ma. This contrasts with the Cascais Platform altitude at 70 m which corresponds to an uplift rate of 0.01 m/ka for the same period.

The UBS13 correlative platform was progressively incised when sea level progressively fell, linked to the development of continental-scale ice sheets in the Northern Hemisphere over the last 2.5 Ma. Since 1
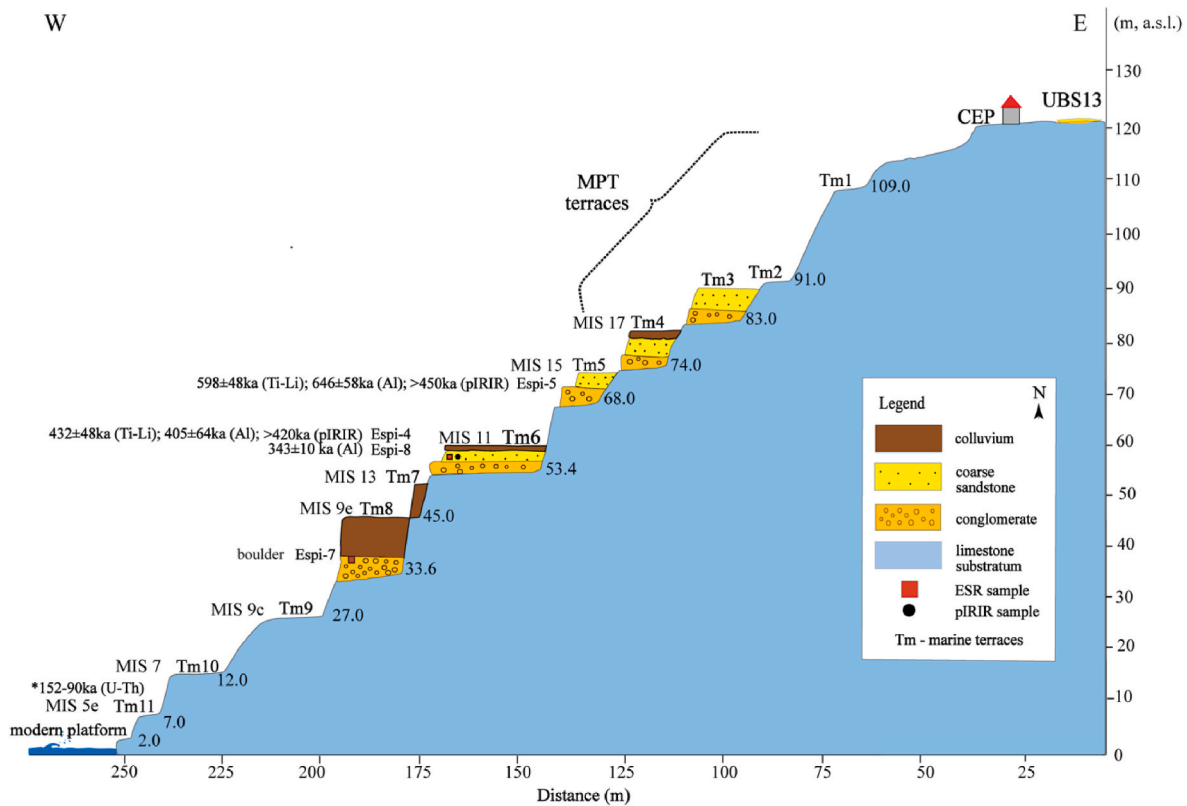
Fig. 11. Schematic cross section of the terrace staircase at Cape Espichel promontory. MPT - Middle Pleistocene Transition.

Ma, continuous uplift was marked by climatic oscillations (glacials and interglacials) with a tendency for cooling and resulting sea-level lowering, generating the staircases of marine terraces.

Comparing the Cape Espichel area with the Cape Raso – Abano beach area (Table 7), the following details can be noted.

a) The marine terraces are more numerous at Cape Espichel than at the Cape Raso – Abano beach area, because at Cape Espichel the uplift rates are high enough to prevent the terraces from being reworked by subsequent high sea levels, except the MIS 13 terrace, which may have been submerged by the high sea level peak of MIS 11.
b) The differential uplift between the two coastal stretches increases with the age of the terraces, from a minimum of 3 m for MIS 7 up to ~34 m for MIS 15-13, reaching 73 - 48 m (145 - 72 m) between the CEP and the CP, using the lower, outer limits of the two platforms.
c) The same difference is reflected on the estimated uplift rates. For example, considering as geomorphic reference the culminant shore platform (3.7 Ma), for the Espichel W promontory the estimated long-term uplift rate is ~0.03 m/ka wile for the Cape Raso is ~0.01 m/ka. Using the marine terrace platform considered as produced by the MIS 15 high stand (572 ka), the estimated uplift rate for Espichel is ~0.13 m/ka, but for the Cape Raso - Abano beach area is ~0.07 m/ka. The terrace staircase at the Cape Espichel promontory also allows to deduce that the estimated uplift rate was nearly constant from ~600 ka to ~200 ka ago (~0.13–0.11 m/ka) but then decreases (0.06–0.01 m/ka).

The physical features of the Portuguese west coast diverge from other passive continental margins, such as the ones of the Western Atlantic, in North America. For instance, on the west coast of Portugal, sandy beaches and offshore barrier islands do not dominate. Rather, rocky coasts formed by erosion, such as headlands and steep sea cliffs, predominate. The geodynamic framework of Iberia is being subjected to strong intraplate compression due to the Africa-Europe plates convergence (Ribeiro

et al., 1990; Zitellini et al., 2004; De Vicente et al., 2018). Despite the Iberian margin unique geodynamic framework, comparison with other passive continental margins around the world are useful for exploring and explaining marine terrace heights and uplift rates (Table 8). For this purpose, we use the compilations of Pedoja et al. (2014, 2018), since prior to these works, uplift rates often corresponded to best estimates, as eustatic sea-level changes were not properly accounted for.

It should be noted that on a global scale, the extension and preservation of marine terraces seem to be promoted in coastal stretches with moderate to low uplift rates (Pedoja et al., 2014; Alvarez-Marrón et al., 2008; Muhs et al., 2014). In view of the obtained results, despite the differences in the number of terraces, elevations and ages, the staircases of Cape Espichel and Cape Raso – Abano beach areas are in agreement with the global coastal sections of moderate to low uplift. Indeed, the uplift rates estimated for the studied middle and upper Plistocene marine terraces are low (0.13–0.01 m/ka), especially when compared to values of 2 m/ka observed in the vicinity of convergent or transform plate boundaries.

Table 8 highlights that the average rates estimated for the two studied stretches of the Portuguese coast are similar to those observed at the northern sector of the Iberian Peninsula, where the culminant shore platform (Rasa) records uplift rates varying between 0.07 m/ka and 0.015 m/ka (Alvarez-Marrón et al., 2008).

On the NW coast of Portugal, with higher uplift, the RSL marker of MIS 5 is found at 2.0–5.5 m a.s.l., the MIS 7 at 7.3–9.3 m and the MIS 9 at ca. 13 m (Carvalhido et al., 2014). However, at the Castelejo beach (SW coast of Portugal), a marine sedimentary terrace located within the present intertidal zone provided two OSL dates of 112 ± 7 ka and 110 ± 5 ka, indicating MIS 5 (Figueiredo, 2015).

In the Cotentin Peninsula (Normandy, France), the MIS 5e benchmark is at 5 ± 1 m and MIS 7 is at 12 m (Pedoja et al., 2018). Both sea level markers are at similar elevations of the same geomorphic markers at Cape Espichel.

Why has the rate of tectonic uplift apparently decreased over the last

Table 8
Coastal uplift rates and elevation of the MIS 1, MIS 5e, MIS 7, MIS 9 and MIS 11 geomorphic markers in different continental passive margins (modified from Pedoja et al., 2014, 2018). In the Cape Raso – Abano beach and Espichel areas, the paleo sea-level changes were incorporated into the uplift rate calculations. * Average uplift rate in short span of time (last 122 ka).

	Domain	MIS 1 (El. m)	MIS 5e (El. m)	MIS 7 (El. m)	MIS 9 (El. m)	MIS 11 (El. m)	Uplift rate (m/ka)
Passive margin	East South America	6.3 ± 1.1	13.1 ± 1.7			50 ± 4	0.11 to 0.01 ± 0.01
	Australia	2 ± 1	7.6 ± 1.1			26.0 ± 1.0	0.06–0.07 ± 0.01
	West Europe	–	6.8 ± 2.0			31.0 ± 1.0	0.06 ± 0.02
	Arabia	2.0 ± 1.2	7.4 ± 2.0			–	0.06 ± 0.02
	Africa West & South	3.5 ± 0.9	6,4 ± 1.1			–	0.05 ± 0.01
	Africa East	3.1 ± 0.5	6.5 ± 1.0			–	0.05 ± 0.01
	East North America	–	6.4 ± 1.1			15.0 ± 1.0	0.05 ± 0.01
	North Mediterranean	–	3.8 ± 1.9			43.3 ± 1.0	0.03 to 0.11 ± 0.01
	Alaska	–	8.6 ± 1.6			23.0 ± 1.0	0.07 ± 0.01
	Normandy (Fr.)	–	5.0 ± 1.0	12 ± 2	22	29 ± 3	0.06 ± 0.01
	Canary Islands		12 to 8			20	0.0 to 0.05
	Cape Raso	2.0	–		22.0		0.04–0.07
	Cape Espichel	2.0	7.0	12.0	33.6	53.4	0.01*to 0.13

~200 ka in the studied coastal stretch of Iberia? Subsidence due to glacial isostatic adjustment (GIA) after the Last Glacial Maximum (LGM) does not explains the relatively low elevation of the MIS 5e marine terrace in Cape Espichel (+7 m) as previous peripheral forebulge uplift had to be compensated. Actually, subsidence rates of −0.5 to −1 m/ka due to GIA have been predicted for the study region (Serpelloni et al., 2013), and present, short term, GPS based, vertical geodetic velocity rates in the study region of ~0 mm/yr (Serpelloni et al., 2013) and rates corrected for GIA also close to 0 mm/yr (Faccenna and Becker, 2020) have been estimated. As GIA does not explain the unexpected low height of the marine platforms ascribed to the MIS 5, a combination of active tectonics and deep-seated geodynamic processes must be invoked, mantle dynamics being the most likely process.

7. Conclusions

The geomorphological and geochronological data obtained from the studied shore platforms cut into resistant limestones and their associated coastal deposits, confirm the action of high energy coastal marine processes (erosion and sedimentation) during periods of high sea level, under low to moderate uplift rate conditions.

The studied geomorphic references (shore platforms) at the Cape Espichel area are more elevated than the coeval references at the Cape Raso – Abano beach area, indicating differential uplift between the two areas. Indeed, considering the regional culminant shore platform (3.7 Ma), for the Cape Espichel promontory the estimated long-term uplift rate is ~0.03 m/ka while for the Cape Raso – Abano beach area it is only ~0.01 m/ka. Also, by using the marine terrace platform considered as produced by the MIS 15 high stand (572 ka), the estimated uplift rate for the west end of Espichel Cape is ~0.13 m/ka, while for the Cape Raso – Abano beach area it is ~0.07 m/ka. The terrace staircase at the Cape Espichel promontory also allows to deduce that the estimated uplift rate was nearly constant during ~600 ka to ~200 ka ago (~0.13–0.11 m/ka), but it after decreases (0.06–0.01 m/ka).

Our study supports that the sequential correlation between marine terrace elevation and different MIS can be problematic if a robust numerical dating framework is not available.

CRediT authorship contribution statement

António A. Martins: Writing – original draft, Conceptualization. **Margarida P. Gouveia:** Writing – original draft, Investigation, Formal analysis, Data curation. **Pedro P. Cunha:** Writing – original draft, Investigation, Formal analysis, Data curation, Conceptualization. **João Cabral:** Writing – original draft, Supervision, Investigation. **Alberto Gomes:** Writing – original draft, Visualization, Investigation. **Christophe Falguères:** Software, Methodology, Investigation. **Pierre Voinchet:** Software, Methodology, Investigation, Conceptualization. **Martin Stokes:** Writing – original draft, Investigation. **Bento Caldeira:** Software. **Jan-Pieter Buylaert:** Methodology, Formal analysis. **Andrew S. Murray:** Methodology, Formal analysis. **Jean-Jacques Bahain:** Software, Methodology. **Silvério Figueiredo:** Investigation.

Disclosure statement

No potentipal conflict of interest was reported by the authors.

Declaration of competing interest

The authors declare that they have no known competing financial interests or personal relationships that could have appeared to influence the work reported in this paper.

Acknowledgments

Appendix A. Supplementary data

Supplementary data to this article can be found online at https://doi.org/10.1016/j.quaint.2024.109657.

References

Alvarez-Marrón, J., Hetzel, R., Niedennann, S., Menendez, R., Marquinez, J., 2008. Origin, structure and exposure history of a wave-cut platform more than 1 Ma in age at the coast of northern Spain: a multiple cosmogenic nuclide approach. Geomorphology 93, 316–334.

Anderson, R.S., Densmore, A.L., Ellis, M.A., 1999. The generation and degradation of marine terraces. Basin Res. 11 (1), 7–19. https://doi.org/10.1046/j.1365-2117.1999.00085.x.

Araújo, M.A., 1991. Evolução Geomorfológica da Plataforma Litoral da região do Porto. Physical Geography, FLUP. Porto University, p. 534. Ph.D. Thesis.

Araújo, M.A., 2008. Depósitos do Pleistocénico Superior e do Holocénico na Plataforma Litoral da Região do Porto: a Morfologia das Plataformas de Erosão Marinha e a Tectónica Recente. Estudos do Quaternário 5, 17–30. APEQ.

Araújo, M.A., 2020. A northwest Portuguese coast: a longitudinal coastline and its diversity. In: Vieira, G., Zêzere, J., Mora, C. (Eds.), Landscapes and Landforms of Portugal. World Geomorphological Landscapes. Springer, Cham, pp. 83–98. https://doi.org/10.1007/978-3-319-03641-0_8.

Bloom, A.L., Yonekura, N., 1990. Graphic analysis of dislocated Quaternary shorelines. Sea-level change. Studies in Geophysics. Natl. Academic press, Washington, dc, pp. 104–115.

Brennan, B.J., 2003. Beta doses to spherical grains. Radiat. Meas. 37 (4–5), 299–303.

Brennan, B.J., Lyons, R.G., Philips, S.W., 1991. Attenuation of alpha particle track dose for spherical grains. Int. J. Radiat. Appl. Instrum. Part D. Nucl. Tracks Radiat. Meas. 18, 249–253.

Breuil, H., Vaultier, M., Zbyszewski, G., 1942. Les plages anciennes portugaises entre le cap d'Espichel et la presqu'île de Peniche et leurs industries paléolithiques. In: Comptes rendus des séances de l'Académie des Inscriptions et Belles-Lettres, 86e année, pp. 102–109. https://doi.org/10.3406/crai.1942.77511, 2-3, 1942.

Breuil, H., Zbyszewsky, G., 1945. Contribution à l'étude des industries paléolithiques du Portugal et leur rapports avec la géologie du Quaternaire. Les principaux gisements des plages quaternaires du litoral d'Estremadura et des terrasses fluviales de la basse vallée du Tage. Comum. Serviços Geol. de Portugal, t. XXVI. II, p. 662.

Cabral, J., 1995. Neotectónica em Portugal continental. Memórias do Instituto Geológico e Mineiro 31, 265p.

Cachão, M., 1990. Posicionamento biostratigráfico da jazida pliocénica de Carnide (Pombal). Gaia 2, 11–16. Lisboa.

Carvalhido, R., Pereira, D., Cunha, P., Jan-Pieter, B., Murray, A., 2014. Characterization and dating of coastal deposits of NW Portugal (Minho- Neiva area): a record of climate, eustasy and crustal uplift during the Quaternary. Quat. Int. 328–329, 94–106.

Creveling, J., Mitrovica, J., Hay, C.C., Austermann, J., Kopp, R.E., 2015. Revisiting tectonic corrections applied to Pleistocene sea-level highstands. Quat. Sci. Rev. 111, 72–80. https://doi.org/10.1016/j.quascirev.2015.01.003.

Creveling, J., Mitrovica, J., Clark, P., Waelbroeck, C., Tamara, P., 2017. Predicted bounds on peak global mean sea level during marine isotope stages 5a and 5c. Quat. Sci. Rev. 163, 193–208.

Cunha, P.P., 2019. Cenozoic basins of western Iberia: mondego, lower tejo and alvalade basins. In: Quesada, C., Oliveira, J.T. (Eds.), The Geology of Iberia: A Geodynamic Approach. Regional Geology Reviews, Springer International Publishing, vol. 4. Cenozoic Basins, Chapter 4, pp. 105–130. https://doi.org/10.1007/978-3-030-11190-8. Hardcover ISBN 978-3-030-11190-8; 184.

Cunha, P.P., Barbosa, B.P., Pena dos Reis, R., 1993. Synthesis of the piacenzian onshore record, between the aveiro and setúbal parallels (western Portuguese margin). Cien. Terra 12, 35–43.

Cunha, P.P., Martins, A.A., Cabral, J., Gouveia, M.P., Buylaert, J.-P., Murray, A.S., 2015. Staircases of wave-cut platforms in western central Portugal (Cape Mondego to Cape Espichel) – relevance as indicators of crustal uplift. Escadarias de terraços marinhos em Portugal centro-ocidental (Cabo Mondego ao Cabo Espichel) – relevância como indicadores de soerguimento crustal. Resúmenes sobre el VIII Simposio MIA15, Málaga del 21 al 23 de Septiembre de 2015, pp. 141–144.

Cunha, P.P., Martins, A.A., Gomes, A., Stokes, M., Cabral, J., Lopes, F., Pereira, D., De Vicente, G., Buylaert, J.-P., Murray, A.S., Antón, L., 2019. Mechanisms and age estimates of continental-scale endorheic to exorheic drainage transition: douro River, Western Iberia. Global Planet. Change 181, 102985. https://doi.org/10.1016/j.gloplacha.2019.102985.

Choffat, P., Dollfus, G.F., 1904/1907. Quelques cordons littoraux marins du Pléistocène du Portugal. Comunicações da Comissão dos Serviços Geológicos de Portugal. Lisboa 6, 158–173.

Daveau, S., Azevedo, T.M., 1980. Aspectos da evolução do relevo da extremidade sudoeste da Arrábida (Portugal). Boletim Sociedade Geológica Portugal, volume de homenagem ao Prof. Carlos Teixeira 163–180.

Dias, M.H., 1980. A Plataforma litoral a norte de Sintra. Estudo dos depósitos de cobertura. Linha de Acção de Geografia Fisica, Relatório n.° 11. Centro de Estudos Geográficos, Lisboa.

De Vicente, G., Cunha, P.P., Muñoz-Martín, A., Cloetingh, S.A.P.L., Olaiz, A., Vegas, R., 2018. The Spanish-Portuguese central system: an example of intense intraplate deformation and strain partitioning. Tectonics 37, 4444–4469. https://doi.org/10.1029/2018TC005204.

De Santis, V., Scardino, G., Scicchitano, G., Meschis, M., Montagna, P., Pons-Braanchu, E., Ortiz, J.E., Sanchez-Palencia, Y., Caldara, M., 2023. Midle-late Pleistocene chronology of paleshorelines and uplift history in the low-rising to stable Apulian foreland: overprinting and reoccupation. Geomorphology 421, 108530. https://doi.org/10.1016/j.geomorph.2022.108530.

Dumitru, O.A., Austermann, J., Polyak, V.J., et al., 2021a. Sea-level stands from the Western Mediterranean over the past 6.5 million years. Sci. Rep. 11, 261. https://doi.org/10.1038/s41598-020-80025-6.

Diniz, F., 1984. Apports de la palynologie à la connaissance du Pliocene Portugais. Rio Maior, un bassin de reference pour l' histoire de la flore, de la vegetation et du climat de la façade atlantique de l' Europe meridionale. These, Univ. Sc. Techn. Languedoc. 230. Montpellier.

Diniz, F., Silva, C.M., Cachão, M., 2016. O Pliocénico de Pombal (Bacia do Mondego, Portugal oeste): biostratigrafia, paleoecologia e paleobiogeografia. Estudos do Quaternário 14, 41–59.

Dowsett, H.J., 2007. The PRISM Palaeoclimate reconstruction and Pliocene sea-surface temperature. In: Williams, M., Haywood, A.M., Gregory, J., Schmidt, D.N. (Eds.), Deep-Time Perspectives on Climate Change: Marrying the Signal from Computer Models and Biological Proxies, The Micropalaeontological Society. Special Publications, The Geological Society, London, UK, pp. 459–480.

Duarte, D., Volochay, K., Magalhães, R., Amaro, S., Cabral, J., 2014. Caracterização de terraços marinhos entre Cascais e o Cabo da Roca, com recurso a elementos cartográficos e de detecção remota. Implicações Neotectonicas. Geonovas 27, 39–46.

Dumitru, O.A., Austermann, J., Polyak, V.J., Fornos, J.J., Asmeron, Y., Ginés, J., Ginés, A., Onac, B.P., 2021b. Sea-level stands from the Western Mediterranean over the past 6.5 million years. Sci. Rep. 11, 261. https://doi.org/10.1038/s41598-020-80025-6.

Duval, M., Grün, R., Falguères, C., Bahain, J.J., Dolo, J.M., 2009. ESR dating of Lower Pleistocene fossil teeth: limits of the single saturating exponential (SSE) function for the equivalent dose determination. Radiat. Meas. 44 (5–6), 477–482. https://doi.org/10.1016/j.radmeas.2009.03.017.

Duval, M., Bahain, J.J., Bartz, M., Falgueres, C., Guilarte, V., Moreno-García, D., Arnold, L.J., 2017. Defining minimum reporting requirements for ESR dating of optically bleached quartz grains. Ancient TL 35 (1), 11–19.

Erlides, Equipa, 1992. – Découverte d'un niveau marin submergé le long de la chaîne de l'Arrábida. Finisterra 53–54, 183–186.

Faccenna, C., Becker, T.W., 2020. Topographic expressions of mantle dynamics in the Mediterranean. Earth Sci. Rev. 209, 103327. https://doi.org/10.1016/j.earscirev.2020.103327. ISSN 0012-8252.

Ferreira, A.B., 2005. Geografia de Portugal, vol. I. O Ambiente Físico, Circulo de Leitores, Lisboa.

Ferreira, A.B., 1983. Problemas de evolução geomorfológica quaternária do noroeste de Portugal, Cadernos do Laboratório Xeolóxico de Laxe, 5, VI Reunion do Grupo Español de Trabalho do Quaternario, A Coruña, 311-330.

Ferreira, A.B., 1991. Neotectonics in Northern Portugal – geomorphological approach. Z. Geomorph NF (Supl·Bd 82) 73–85.

Figueiredo, P., 2015. Neotectonics of the Southwest Portugal Mainland: Implications of the Regional Seismic Hazard. Doctoral dissertation, Universidade de Lisboa, 261pp.

Figueiredo, P., Cabral, J., Rockwell, T., 2013. Recognition of Pleistocene marine terraces in the southwest of Portugal (Iberian Peninsula): evidences of regional Quaternary uplift. Ann. Geophys. 56 (6), 2013. https://doi.org/10.4401/ag-6276. S0672.

Fonseca, A.F., Zêzere, J.L., Neves, M., 2014. Geomorphology of the Arrábida chain (Portugal). J. Maps 10 (1), 103–108. https://doi.org/10.1080/17445647.2013.859637.

Fonseca, A.F., Zêzere, J.L., Neves, M., 2015. Contribution to the knowledge of the geomorphology of the Arrábida Chain (Portugal): geomorphological mapping and geomorphometry. Rev. Bras. Geomorfologia 16 (1), 137–163.

Fonseca, A.F., Zêzere, J.L., Neves, M., 2020. The Arrábida chain: the alpine orogeny in the vicinity of the Atlantic Ocean. In: Vieira, G., Zêzere, J., Mora, C. (Eds.), Landscapes and Landforms of Portugal. World Geomorphological Landscapes. Springer, Cham. https://doi.org/10.1007/978-3-319-03641-0_21.

Gouveia, M.P., Cunha, P.P., Falguères, C., Voinchet, P., Martins, A.A., Bahain, J.-J., Pereira, A., 2020. Electron spin resonance dating of the culminant allostratigraphic unit of the Mondego and Lower Tejo Cenozoic basins (W Iberia), which predates fluvial incision into the basin-fill sediments. Global Planet. Change 184, 103081. https://doi.org/10.1016/j.gloplacha.2019.103081, 1-14.

Granja, H., De Groot, T., Costa, A., 2008. Evidence for Pleistocene wet aeolian dune and interdune accumulation, S. Pedro da Maceda, north-west Portugal. Sedimentology 55, 1203–1226.

Grün, R., 1994. A cautionary note: use of the water content and depth for cosmic ray dose rate in AGE and DATA programs. Ancient TL 12, 50–51.

Guérin, G., Mercier, N., Adamiec, G., 2011. Dose-rate conversion factors: update. Ancient TL 29, 5–8.

Hearty, P.J., Rovere, A., Sandstrom, M.R., O'Leary, M.J., Roberts, D., Raymo, M.E., 2020. Pliocene-Pleistocene stratigraphy and sea-level estimates, Republic of South Africa with implications for a 400 ppmv CO2 world. Paleoceanogr. Paleoclimatol. 35, e2019PA003835. https://doi.org/10.1029/2019PA003835.

Kullberg, M.C., Kullberg, J.C., 2000. Tectónica da Região de Sintra. Tectónica das regiões de Sintra e Arrábida. Mem, Geociências 2, 1–34. Universidade de Lisboa.

Kullberg, J.C., Kullberg, M.C., 2017. The tectono-stratigraphic evolution of an Atlantic-type basin: an example from the Arrábida sector of the Lusitanian Basin. Ciências da Terra - Earth Sciences Journal 19 (1), 55–74.

Kullberg, M.C., Kullberg, J.C., Terrinha, P., 2000. Tectónica da Cadeia da Arrábida. Tectónica das regiões de Sintra e Arrábida, Memórias Geociências 2, 35–84. Museu Nac Hist Nat Univ Lisboa.

Kullberg, M.C., Kullberg, J.C., 2020. Landforms and Geology of the Serra de Sintra and Its surroundings. In: Vieira, G., Zêzere, J., Mora, C. (Eds.), Landscapes and Landforms of Portugal. World Geomorphological Landscapes. Springer, Cham. https://doi.org/10.1007/978-3-319-03641-0_19.

Lajoie, K.R., 1986. Coastal tectonics. In: Usselman, T.M. (Ed.), Studies in Geophysics, ActiveTectonics. National Academy Press, Washington DC, pp. 95–124.

Manuppella, G., Antunes, M.T., Pais, J., Ramalho, M.M., Rey, J., 1999. Carta geológica de portugal na escala 1:50000. Notícia explicativa da folha 38-B Setúbal. Instituto Geológico e Mineiro, p. 143.

Merrits, D., Bull, W.B., 1989. Interpreting Quaternary uplift rates at the Mendocino triple junction, northern California, from uplifted marine terraces. Geology 17 (11), 1020–1024.

Miller, K.G., Wright, J., Browning, J., Kulpecz, A., Kominz, M., Naish, T., Cramer, B., Rosenthal, Y., Peltier, W., Sosdian, S., 2012. High tide of the warm Pliocene: implications of global sea level for Antarctic deglaciation. Geology 40, 407–410.

Miller, K.G., Browning, J.V., Schmelz, W.J., Kopp, R.E., Mountain, G.S., Wright, J.D., 2020. Cenozoic sea-level and cryospheric evolution from deep-sea geochemical and continental margin records. Sci Adv. 2020 May 15 6 (20), eaaz1346. https://doi.org/10.1126/sciadv.aaz1346. PMID: 32440543; PMCID: PMC7228749.

Monge-Soares, A., Moniz, C., Cabral, J., 2006. A Duna Consolidada de Oitavos (a Oeste de Cascais - Regiao de Lisboa) - a sua Datação pelo Método do Radiocarbono The Consolidated Dune of Oitavos (west of Cascais - Lisbon Region) - its Dating by the Radiocarbon Method. Comunicações Geológicas 93, 105–118.

Moniz, C., 2010. Contributo para o conhecimento da falha de Pinhal Novo-Alcochete, no âmbito da neotectónica do vale inferior do Tejo (Doctoral dissertation).

Mörner, N., 1982. Sea level curves. Beaches and coastal Geology. Encyclopedia of Earth Sciences Series. Springer, New York, NY. https://doi.org/10.1007/0-387-30843-1_399.

Muhs, D.R., Pandolfi, J.M., Simmons, K.R., Scumann, R.R., 2012. Sea-level history of past interglacial periods from uranium-series dating of corals, Curaçao, Leeward Antilles islands. Quaternary Research 78 (2), 157–169.

Muhs, D., Meco, J., Simmons, K., 2014. Uranium-series ages of corals, sea level history, and palaeozoogeography, Canary Islands, Spain: an exploratory study for two Quaternary interglacial periods. Palaeogeogr. Palaeoclimatol. Palaeoecol. 394, 99–118.

Murray, A., Marten, R., Johnston, A., Martin, P., 1987. Analysis for naturally occurring radionuclides at environmental concentrations by gamma spectrometry. J. Radioanal. Nucl. Chem. 115, 263–288.

Pais, J., Legoinha, P., 2000. Gruta da Figueira Brava (Arrábida): Geological Setting. Memórias da Academia das Ciências de Lisboa, Classe de Ciências, tomo XXXVIII, pp. 69–81.

Pedoja, K., Husson, L., Johnson, M.E., Melnick, D., Witt, C., Pochat, S., Nexer, M., Delcaillau, B., Pinegina, T., Poprawski, Y., Authemayou, C., Elliot, M., Regard, V., Garestier, F., 2014. Coastal staircase sequences reflecting sea-level oscillations and tectonic uplift during the Quaternary and Neogene. Earth Sci. Rev. 132, 13–38. https://doi.org/10.1016/j.earscirev.2014.01.007.

Pedoja, K., Jara-Muñoz, J., De Gelder, G., Robertson, J., Meschis, M., Fernandez-Blanco, D., Nexer, M., Poprawski, Y., Dugué, O., Delcaillau, B., Bessin, P., Benabdelouahed, M., Authemayou, C., Husson, L., Regard, V., Menier, D., Pinel, B., 2018. Neogene-Quaternary slow coastal uplift of Western Europe through the perspective of sequences of strandlines from the Cotentin Peninsula (Normandy, France). Geomorphology 303, 338–356. https://doi.org/10.1016/j.geomorph.2017.11.021.

Pirazzoli, P.A., Radtke, U., Hantoro, W.S., Jouannic, C., Hoang, C.T., Causse, C., Borel Best, M., 1993. A one million-year-long sequence of marine terraces on Sumba Island, Indonesia. Mar. Geol. 109, 221–236.

Prescott, J.R., Hutton, J.T., 1994. Cosmic ray contributions to dose rates for luminescence and ESR dating: large depths and long-term time variations. Radiat. Meas. 23, 497–500.

Prudêncio, M.I., Marques, R., Rebelo, L., Cook, G.T., Cardoso, G.O., Naysmith, P., Freeman, S.T., Franco, D., Brito, P., Dias, M.I., 2007. Radiocarbon and blue optically stimulated luminescence chronologies of the Oitavos consolidated dune (Western Portugal). Radiocarbon 49 (2), 1145–1151.

Ramos, A., Cunha, P.P., Cunha, L., Gomes, A., Lopes, F.C., Buylaert, J.-P., Murray, A.S., 2012. The River Mondego terraces at the Figueira da Foz coastal area (western central Portugal): geomorphological and sedimentological characterization of a terrace staircase affected by differential uplift and glacio-eustasy. Geomorphology 165–166, 107–123. https://doi.org/10.1016/j.geomorph.2012.03.037.

Ramos-Pereira, A., 2008. Sea Level Changes and Neotectonics: Some Examples in Portugal (Arrábida and Southwest), vol. 5. Estudos do Quaternário, APEQ, Porto, pp. 31–37, 2008.

Ramos-Pereira, A., Regnauld, H., 1994. Litorais quaternários (emersos e submersos) na extremidade sudoeste da Arrábida (Portugal). In: Ramos Pereira, A., et al. (Eds.), Contribuições para a geomorfologia e dinâmicas litorais em Portugal, vol. 35. Centro de Estudos Geográficos, Linha de Acção de Geografia Física, pp. 55–73.

Ramos-Pereira, A., Angelucci, D., 2004. Formações dunares no litoral português, do final do Plistocénico e inícios do Holocénico, como indicadores paleoclimáticos e paleogeográficos. In: Tavares, A.A., Tavares, M.J., Cardoso, J.L. (Eds.), Evolução Geohistórica da Litoral Português e Fenómenos Correlativos. Universidade Aberta, pp. 221–256.

Ramos-Pereira, Neves, M., Trindade, J., Borges, B., Angelucci, D., Monge-Soares, A., 2007. Dunas carbonatadas e depósitos correlativos na Estremadura (Portugal). Variações do nível do mar e neotectónica. Publicações da Associação Portuguesa de Geomorfólogos 5, 165–168. APGeom, Lisboa.

Ramos-Pereira, A., Ramos, C., 2020. The Southwest coast of Portugal. In: Vieira, G., Zêzere, J., Mora, C. (Eds.), Landscapes and Landforms of Portugal. World Geomorphological Landscapes. Springer, Cham. https://doi.org/10.1007/978-3-319-03641-0_8.

Raymo, M.E., Hearty, P., De Conto, R., O'Leary, M., Dowsett, H.J., Robinson, M.M., Mitrovica, J.X., 2009. PLIOMAX: Pliocene maximum sea level project. Science Highlights: Paleo Sea Level 17 (2), 58–59. https://doi.org/10.22498/pages.17.2.58.

Raymo, M.E., Kozdon, R., Evans, D., Lisiecki, L., Ford, H.L., 2018. The accuracy of mid-Pliocene δ18O-based ice volume and sea level reconstructions. Earth Sci. Rev. 177, 291–302.

Ressurreição, R., 2018. Evolução tectono-estratigráfica cenozóica do litoral alentejano (sector Melides-Odemira) e enquadramento no regime geodinâmico actual. PhD. Thesis. Universidade de Lisboa, Faculdade de Ciências, p. 296.

Ribeiro, A., Kullberg, M.C., Kullberg, J.C., Manupella, G., Phipps, S., 1990. A review of Alpine Tectonics in Portugal: foreland detachment in basement and cover rocks. Tectonophysics 18 (4), 357–366.

Ribeiro, C., 1867. Note sur le terrain quaternaire du Portugal. Bull. Soc. Geol. Fr. 24, 692–717.

Ribeiro, O., 1935. A Arrábida. Esboço geográfico. Dissertação de Doutoramento em Ciências Geográficas. Faculdade de Letras da Universidade de Lisboa, Lisboa, p. 94.

Ribeiro, H., Pinto de Jesus, A., Sanjurjo, J., et al., 2019. Multidisciplinary study of the quaternary deposits of the Vila Nova de Gaia, NW Portugal, and its climate significance. J. Iber. Geol. 45, 553–563. https://doi.org/10.1007/s41513-019-00109-9.

Ribeiro, O., 1940. Remarques sur la morphologie de la région de Sintra et Cascais. Rev. Géograph Pyrénées Sud-Ouest II 3–4, 203–218.

Ribeiro, O., 1968. Excursão à Arrábida. Finisterra III (6), 257–273. Lisboa.

Roberts, G.P., Houghton, S.L., Underwood, C., Papanikolaou, I., Cowie, P.A., Van Calsteren, P., Wigley, T., Cooper, F.J., McArthur, J.M., 2009. Localization of Quaternary slip rates in an active rift in 105 years: an example from central Greece constrained by 234Ue230Th coral dates from uplifted paleoshorelines. J. Geophys. Res. 114, B10406. https://doi.org/10.1029/2008JB005818.

Roberts, G.P., Meschis, M., Houghton, S., Underwood, C., Briant, R.M., 2013. The implications of revised Quaternary paleo-shoreline chronologies for the rates of active extension and uplift in the upper plate of subduction zones. Quat. Sci. Rev. 78, 169–187.

Robertson, J., Roberts, G.P., Ganas, A., Meschis, M., Gheorghiu, D.M., Shanks, R.P., 2023. Quaternary uplift of palaeoshorelines in southwestern Crete: the combined effect of extensional and compressional faulting. Quat. Sci. Rev. 316, 108240. https://doi.org/10.1016/j.quascirev.2023.108240.

Rowe, M.P., Wainer, K.A., Bristow, C.S., Thomas, A.L., 2014. Anomalous MIS 7 sea level recorded on Bermuda. Quat. Sci. Rev. 90, 47–59.

Serpelloni, E., Faccenna, C., Spada, G., Dong, D., Williams, S.D.P., 2013. Vertical GPS ground motion rates in the Euro-Mediterranean region: new evidence of velocity gradients at different spatial scales along the Nubia-Eurasia plate boundary. J. Geophys. Res. Solid Earth 118. https://doi.org/10.1002/2013JB010102.

Spratt, R.M., Lisiecki, L.E., 2016. A Late Pleistocene sea level stack. Clim. Past 12 (4), 1079–1092. http://www.clim-past.net/12/1079/2016/doi:10.5194/cp-12-1079-2016-supplement.

Stevens, T., Buylaert, J.-P., Thiel, C., et al., 2018. Ice-volume-forced erosion of the Chinese Loess Plateau global Quaternary stratotype site. Nat. Commun. 9, 983.

Teixeira, C., 1979. Plio-Plistocénico de Portugal. Com. Serv. Geol. Portugal 35–46. Lisboa, LXV.

Vandenberghe, D., De Corte, F., Buylaert, J.-P., Kučera, J., Van den haute, P., 2008. On the internal radioactivity in quartz. Radiation Measurements. Proceedings of the 15th Solid State Dosimetry (SSD15) 43, 771–775. https://doi.org/10.1016/j.radmeas.2008.01.016.

Voinchet, P., Yin, G., Falguères, C., Liu, C., Han, F., Sun, X., Bahain, J., 2013. ESR dose response of Al center measured in quartz samples from the Yellow River (China): implications for the dating of Upper Pleistocene sediment. Geochronometria 40 (4), 341–347.

Yokoyama, Y., Falguères, C., Quaegebeur, J.P., 1985. ESR dating of quartz from Quaternary sediments: first attemps. Nucl. Tracks 10 (4–6), 921–928.

Zhao, H., Li, S.H., 2005. Internal dose rate to K-feldspar grains from radioactive elements other than potassium. Radiation Measurements 40 (1), 84–93.

Zilhão, J., Angelucci, D.E., Araújo Igreja, M., Arnold, L.J., Badal, E., Callapez, P., Cardoso, J.L., d'Errico, F., Daura, J., Demuro, M., Deschamps, M., Dupont, C., Gabriel, S., Hoffmann, D.L., Legoinha, P., Matias, H., Monge Soares, A.M., Nabais, M., Portela, P., Queffelec, A., Rodrigues, F., Souto, P., 2020. Last interglacial iberian neandertals as Fisher-hunter-gatherers. Science 367 (1443), 1–13. https://doi.org/10.1126/science.aaz7943.

Zitellini, N., Rovere, M., Terrinha, P., Chierici, F., Matias, L., Bigsets Team, 2004. Neogene through Quaternary tectonic reactivation of SW Iberian passive margin; geodynamics of Azores Tunisia. Pure Appl. Geophys. 161 (3), 565–587. https://doi.org/10.1007/s00024-003-2463-4.